Aerodynamics Flapping-Flight Robotic Bird using Unsteady Lifting-Line Method

Luuk H. Groot Koerkamp[1], HarryW.M. Hoeijmakers[2],
Cees H. Venner[3], Stefano. Stramigioli[4]
University of Twente, Enschede, the Netherlands

The Robird is a bird-like drone or ornithopter, that generates lift and thrust by flapping/pitching its wing, which performance resembles that of a Peregrine falcon. This paper describes an extension from steady flow to unsteady flow of Prandtl's Lifting-line method to predict the unsteady lift, thrust, pitching moment, required power and propulsive efficiency of the robotic bird. The extension comprises the derivation of the Kutta-Joukowski Theorem for unsteady flow, an unsteady Kutta condition and the representation of the wake as a stationary transpiration-type of surface carrying a time-dependent dipole distribution, which instantaneous strength is obtained from the spanwise distribution of the circulation of the lifting line at earlier times. For the cases considered, the numerical method predicts that both the section-lift, section-thrust and section-pitching-moment of the wing vary with time. The cycle-averaged section-lift and section-thrust, as well as the cycle-averaged overall lift and thrust, are mostly positive during the flapping flight. The spanwise distributions of cycle-averaged sectional circulation, lift, pitching-moment and upwash, as well as cycle-averaged overall lift and pitching-moment depend on Strouhal number, not on pitch amplitude, whereas the spanwise distribution of cycle-averaged sectional thrust and required power, as well as cycle-averaged overall thrust, required power and propulsive efficiency depend on Strouhal number and on pitch amplitude. The topology of the wake in terms of the unsteady wake dipole and its corresponding vortex distribution as predicted by the unsteady-lifting-line method, depends on Strouhal number and amplitude of the pitching motion. The paper describes the relation between wake topology and the generation of lift and thrust.

I. Introduction

The Robird [1] is an ornithopter-type of drone developed by Clear Flight Solutions (CFS) that, during its flight, was designed to appear like a Peregrine falcon, see Fig. 1. The drone has the same dimensions and weight as the real falcon, and produces lift and thrust by flapping/pitching its wings. Birds instinctively sense that a falcon in flapping flight is on the hunt, making the Robird very suitable for bird control at airports, garbage dumps, crop fields, etc. The foam wings of the Robird differ from the wings of ornithopters of similar size, such as the Robo Raven [2], since it features than airfoil-type wings rather than foil-type wings.

Furthermore, the Robird wings do not pitch passively nor consist of hinged, individually moving, parts like the Festo Smartbird [3]. The size of drones like the Robird, the Robo Raven and the Smartbird, is in a different class than successful flapping Micro-Aerial Vehicles (MAV's), such as the Delfly [4] and the insect-sized robotic fly [5].

The performance of flapping wings is dominated by unsteady flow phenomena, which makes the aerodynamics inherently complex. Experimental work on birds and bird-like flapping wings has shown the importance of mechanisms such as leading-edge vortices for slow flight and hovering flight [6–8]. The challenge of formulating an aerodynamic model for flapping wings is to account for the dynamics of the wake, which is required to accurately predict the aerodynamic performance [9]. Many models for the wake have been proposed in the past [10, 11, 12].

[1] PhD Student, Department Electrical Engineering, Mathematics and Computer Sciences. Student Member AIAA.
[2] Professor, Department Engineering Technology. Senior Member AIAA.
[3] Professor, Department Engineering Technology. Member AIAA.
[4] Professor, Department Electrical Engineering, Mathematics and Computer Sciences.

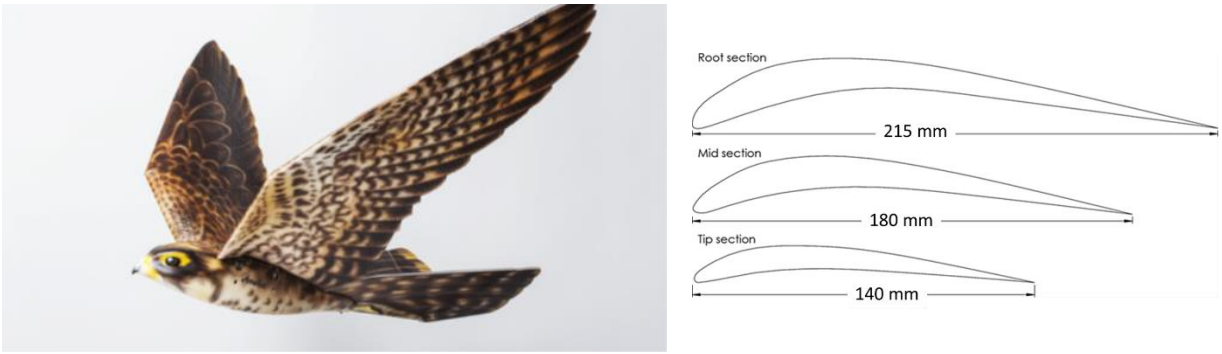

Fig. 1 Robird [1], robotic bird based on Peregrine falcon (left). Typical airfoil sections wing Robird. (right).

The results of these models share one important characteristic: the generation of thrust is associated with a wake that induces a jet-like chordwise flow. This jet-like flow has been confirmed to be present in the wake of the Robird with both numerical methods [13] and experimental methods [14, 15]. The choice of the model of the wake may depend on the bird species, and may even vary with flight speed for specific birds [16]. The accuracy of the wake models is grossly determined by vortex dynamics, which carries over to the accuracy of the prediction of lift and drag. [17].

Though the Robird proves that flapping flight by a robotic bird is possible, the theory behind the aerodynamics of flapping flight is not yet fully understood. The goal of the present study, carried out since 2012, is to contribute to a better understanding of the aerodynamics of flapping wing propulsion of a robotic bird like the Peregrine-falcon based Robird. In [18] the lift curve has been measured of a scale model of the wing of the Robird in order to obtain the lift and drag polar for steady, non-flapping flow conditions. This established the basic aerodynamics of the wing, with its highly cambered thin airfoil sections (similar to the ones of flying machines in the early part of last century), see Fig. 1, for the robotic bird operating at Reynolds numbers in the range of 30×10^4 to 10^5. CFD analysis [13] performed for 2D flow about the heaving/pitching Robird airfoils shown in Fig. 1, gave first insight in the unsteady aerodynamics of such cambered airfoils, as well as the relation between the flow in the wake and the generation of thrust. Further wind-tunnel studies [14, 15, 19] focused on the wake downstream of a (full-scale) half-model of the Robird during flapping motion, using: (i) a wake rake, as well as a 7-hole probe; (ii) flow visualization, and; (iii) PIV (Particle Image Velocimetry) measurements, respectively. In [19] a simple unsteady potential flow model for 2D heaving/pitching motion has been presented developed for investigating whether representing the wake of a flapping wing by a vortex sheet yields the jet-like type of distribution of the axial velocity, generated by a reversed von Kármán vortex street. Such a velocity distribution in the wake is indicative for the generation of thrust by a flapping wing.

For the subsequent experimental part of the study an advanced PIV set-up has been designed and realized for the upgraded Aero-acoustic Wind Tunnel [20] at the University of Twente (open-jet test section $w \times h$ = 0.9m × 0.7m). In [21, 22] the PIV campaign to obtain wake velocity data for the wake of the Robird port-side wing has been pursued further. In addition, an unsteady lifting-line method has been developed for the 3D flow about flapping wings.

The goal of the present paper is to report on further applications of the unsteady lifting-line method to the Robird flapping motion, in a wider range of parameters and include pitching moment, required-power and propulsive efficiency alongside lift and thrust. Furthermore, within the range of parameters considered, the wake topology is analysed and characterised in more detail.

The present paper is structured as follows: Section 2 introduces the Robird, the kinematics of the flapping wing of the Robird and the simplifications that will be made for the computational part of this study. Section 3 describes the computational method followed by section 4 with a description on how the developed lifting-line method for unsteady flow is applied to the Robird. This section is followed by section 5, which describes the results of the numerical method, followed by the conclusions of the present investigation in section 6.

II. Kinematics Flapping Motion Wing Robotic Bird

The motion of a bird has many degrees of freedom. In the present study the description of the motion is restricted to the motion of a rigid wing with just two degrees of freedom: flapping $\gamma(t)$ and pitching $\theta(t)$. In a 2D frame work,

the motion of a chordwise section of the wing is equivalent to a combination of a heaving $\dot{h}(t)$ and a pitching $\theta(t)$ motion, see Fig. 2.

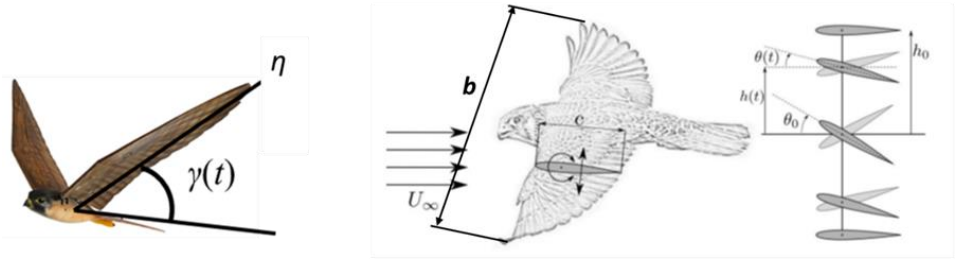

Fig. 2 Flapping/pitching motion of wings [13]. Left: definition flapping motion. Center Free stream velocity and overall dimensions. Right: definition of equivalent 2D heaving/pitching motion airfoil section.

The flapping motion $\gamma(t)$ of the quarter-chord line, is approximated as a harmonic motion of constant period T, defined by

$$\gamma(t) = \gamma_1 + \gamma_0 \sin 2\pi \frac{t}{T}, \tag{1}$$

with $\gamma(t)$ the wing shoulder angle of the pitch axis as function of time, γ_0 is the amplitude of the flapping motion and $\gamma_1$is the zero-position (off-set) of the wing. The period T of the motion equals $T = 1/f$, with f the frequency of the flapping motion. The pitching motion, coupled to the plunging motion, is a harmonic motion, at the same frequency, defined as

$$\theta(t) = \theta_1 + \theta_0 \sin\left(2\pi \frac{t}{T} + \phi\right), \tag{2}$$

with $\theta(t)$ the pitching angle around the pitch axis, here the spanwise quarter-chord line, as function of time, θ_0 the amplitude of the pitch, θ_1 the off-set of the pitch angle (equal to the cycle-averaged pitch angle) and ϕ the phase shift between flapping motion and pitching motion. It is assumed that all motion parameters, i.e., γ_0, γ_1, θ_0, θ_1 and ϕ are constant along the pitch axis.

Note that here the pitch angle θ does not depend on the spanwise coordinate η, i.e., nor geometric twist, nor aerodynamic twist, due to the flexibility of the wing, is considered in the definition of the pitching angle.

The height $h(t)$, above the horizontal plane, of the on-quarter-chord point of the airfoil section at distance y from the pivotal point of the plunging motion, is a function of γ_0 and γ_1:

$$h(y,t) = |y| \sin\gamma(t), \text{ for } y \in [-b/2, b/2], \tag{3}$$

with $b/2$ the semi-span of the wing.

In the lifting-line method to be discussed, the boundary conditions are applied on a stationary reference surface, here the plane $z = 0$. The effect of the motion of the wing is accounted for through the so-called effective angle of attack $\alpha_{eff}(y,t)$ of the airfoil sections along the span of the wing, see Fig. 3:

$$\alpha_{eff}(y,t) = \theta(t) + \arctan\left(\frac{-1}{U_\infty}\frac{\partial h(y,t)}{\partial t}\right). \tag{4}$$

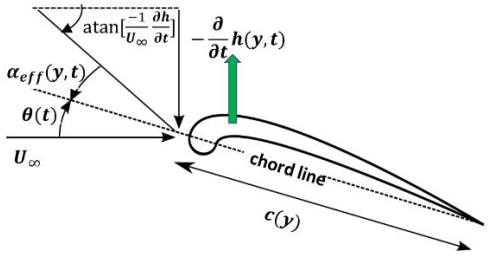

Fig. 3 Effective angle of attack $\alpha_{eff}(y,t)$ due to plunging/pitching motion. Green arrow indicates direction of plunging motion. Angle of attack due to plunging motion equals $\alpha_{plunge} = \arctan\left(\frac{-1}{U_\infty}\frac{\partial h(y,t)}{\partial t}\right.$

The contribution of the plunge (heave) of the airfoil sections due to the flapping motion of the wing follows from the time variation of the position of the flapping/pitching wing with respect to the off-set angle γ_1. With y the distance from the axis of rotation,

$$h(y,t) = |y| \sin(\gamma_1 + \gamma_0 \sin\frac{2\pi t}{T}) \equiv h_1(y) + h_0(y) \sin\left(\frac{2\pi t}{T}\right) \approx |y|\gamma_1 + |y|\gamma_0 \sin\frac{2\pi t}{T}, \tag{5}$$

so that $h_1(y) = |y|\gamma_1$ and $h_0(y) = |y|\gamma_0$. It then follows:

$$\frac{\partial h(y,t)}{\partial t} = |y|\gamma_0 2\pi f \cos\frac{2\pi t}{T}. \tag{6}$$

Substitution in the expression for the effective angle of attack $\alpha_{eff}(y,t)$, given in Eq. (4), yields

$$\alpha_{eff}(y,t) = [\theta_1 + \theta_0 \sin\left(\frac{2\pi t}{T} + \phi\right)] - \arctan\left(\pi \frac{f2|y|\gamma_0}{U_\infty}\cos\frac{2\pi t}{T}\right) \text{ for } y \in [-b/2, b/2]. \tag{7}$$

Note that the angle of attack of the configuration is included in the definition of the effective angle of attack α_{eff}, specifically in θ_1.

In terms of dimensionless quantities, the effective angle of attack of a wing section is expressed as:

$$\alpha_{eff}(\frac{y}{b/2}, \frac{t}{T}) = [\theta_1 + \theta_0 \sin\left(2\pi\frac{t}{T} + \phi\right)] - \arctan\left(\pi \mathrm{St}\frac{|y|}{b/2}\cos 2\pi\frac{t}{T}\right), \tag{8a}$$

with the Strouhal number defined as

$$\mathrm{St} \equiv \frac{f2h_0(y = b/2)}{U_\infty}, \tag{8b}$$

in terms of the arc length, $2h_0(y = b/2) = b\gamma_0$, covered by the wing tip during a full period of the motion. Eq. (8) shows that the effective angle of attack depends on spanwise location $y/0.5b$ and tine t/T, as well as on four independent parameters, i.e.,

$$\alpha_{eff} = \alpha_{eff}(\frac{y}{b/2}, \frac{t}{T}; \theta_1, \theta_0, \phi, \mathrm{St}). \tag{9}$$

For a representative set of parameters, the left plot of Fig. 4 presents the effective angle of attack as function of time, during one cycle, at the tip of the wing $|y|/0.5b = 1$. The right plot of Fig. 4 illustrates the spanwise distribution of the effective angle of attack along the span of the wing, for a number of instants during a cycle.

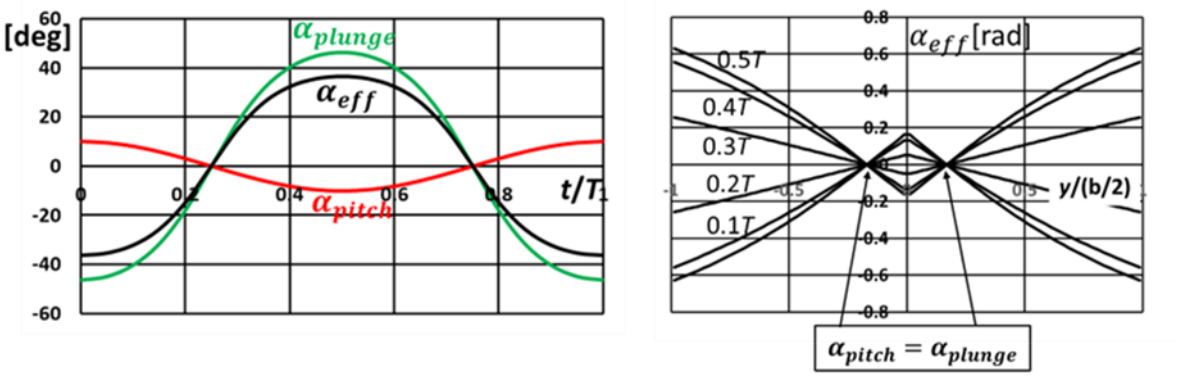

Fig. 4 Effective angle of attack $\alpha_{eff}(|y|/0.5b, t/T)$, in degrees, due to plunging/pitching motion. Left: in radians, as function of t/T at wing tips $|y|/0.5b = 1$. Right: as function of $y/0.5b$ at six instants during half a cycle, from upstroke $t/T \in [0.0.25]$ to downstroke $t/T \in [0.25,0.5]$. $\theta_1 = 0, \theta_0 = 10$ deg, $\phi = 90$ deg, $\mathrm{St} = 0.3343$.

The left plot in Fig. 4 shows that the pitching motion, 90 deg out of phase with the plunging motion, reduces the amplitude of the angle of attack due to the plunge. It shows that, at the wing tips, the effect of the plunge dominates α_{eff}, however, the reduction of α_{eff} by the pitch mitigates the danger of flow separation. Note that, for this set of kinematic parameters, along the whole span, the plunge angle as well as the pitch angle and therefore the effective angle of attack, equal zero at t/T = 0.25 and 0.75 in the cycle, see also the right plot in Fig. 4.

The derivative of $\alpha_{eff}(\frac{y}{b/2}, \frac{t}{T})$ with respect to t/T follows from Eq. (8) as:

$$\frac{\partial}{\partial t}\alpha_{eff}\left(\frac{y}{b/2}, \frac{t}{T}\right) = 2\pi[\theta_0 \cos\left(2\pi\frac{t}{T} + \phi\right) + \frac{\pi \mathrm{St}\frac{|y|}{b/2}\sin 2\pi\frac{t}{T}}{1+\left(\pi \mathrm{St}\frac{|y|}{b/2}\cos 2\pi\frac{t}{T}\right)^2}]. \tag{10}$$

For the case of ϕ = 90 deg, it follows that the derivative equals zero for t/T = 0, 0.5 and 1. The effective angle of attack at the start of the cycle and at the end of the cycle follow as

$$\alpha_{eff}\left(\frac{y}{b/2}, \frac{t}{T}\right) = \theta_1 + \theta_0 - \arctan\left(\pi \mathrm{St}\frac{|y|}{b/2}\right), \text{ at } \frac{t}{T} = 0 \text{ and } 1, \text{ whereas} \tag{11}$$

$$\alpha_{eff}\left(\frac{y}{b/2}, \frac{t}{T}\right) = \theta_1 - \theta_0 + \arctan\left(\pi \mathrm{St}\frac{|y|}{b/2}\right), \text{ at } \frac{t}{T} = 0.5. \tag{12}$$

Therefore, for the present case, at the wing tips, the minimum value of the effective angle of attack $\alpha_{eff,min} = -36.4$ deg at $t/T = 0$ and 1, while the maximum value equals $\alpha_{eff,max} = 36.4$ deg at $t/T = 0.5$. The rather high value of 36.4 deg for the instantaneous effective angle of attack at the wing tips is subject to uncertainties in the measured position of the tips of the (slightly flexible) wing of the wind-tunnel model. For increasing values of θ_0, these maximum and minimum values of α_{eff} decrease in magnitude.

The right plot of Fig. 4 presents the distribution of the effective angle of attack $\alpha_{eff}\left(\frac{y}{\frac{1}{2}b}, \frac{t}{T}\right)$ as function of the spanwise coordinate $\frac{y}{\frac{1}{2}b}$, at six instants in time during half a flapping cycle. Since the angle of attack due to plunging decreases with decreasing y, the effect due to time-dependent part of the pitch and that due to the plunge cancel at a certain value of y along the span of the wing, so that here $\alpha_{eff} = \theta_1$. The spanwise location at which this occurs can be estimated from Eq. (8a) as first-order approximation: $\frac{y}{b/2} \approx \frac{\theta_0}{\pi St}$, at all times. For the present set of parameters, it follows that $|y|/0.5b \approx 0.166$. Subsequently, in the central part of the wing, $\alpha_{eff} = \alpha_{pitch} + \alpha_{plunge}$, changes sign, as is the loading of the inboard sections: the effect of pitching dominates the effective angle of attack. So, for the first half of the flapping cycle, about 1/6-th of the span of the wing features a decreasing α_{eff}, while both outboard panels experience an increasing α_{eff}. For the second half of the cycle this is the other way around. As will be illustrated later, this will be have a clear effect on the topology of the vortex distribution of the wake of the wing.

The expression for $\alpha_{eff}\left(\frac{y}{b/2}, \frac{t}{T}\right)$, Eq. (8), shows that, to first approximation, the effective angle of attack is close to linear in the spanwise coordinate $\frac{|y|}{b/2}$. This is confirmed in the right plot in Fig. 4.

III. Computational Method

In this section the computational method used to determine the lift, thrust, pitching moment and required power of the flapping/pitching wings of the Robird.

A. Governing Equations

In the present study, it is assumed that the flow is inviscid, incompressible, unsteady and irrotational. The latter implies that the vorticity $\vec{\omega} \equiv \vec{\nabla} \times \vec{u} = \vec{0}$ in the whole flow field, but for regions of infinitesimal extent. This enables the introduction of velocity potential $\Phi(x, y, z, t)$, such that $\vec{u}(x, y, z, t) \equiv \vec{\nabla}\Phi(x, y, z, t)$, which satisfies the irrotationality condition implicitly. For incompressible flow the continuity equation reduces to the condition that the flow is divergence-free: $\vec{\nabla}.\vec{u} = 0$. Therefore $\nabla^2\Phi = 0$, i.e., the velocity potential $\Phi(x, y, z, t)$ satisfies Laplace's equation:

$$\frac{\partial^2\Phi}{\partial x^2} + \frac{\partial^2\Phi}{\partial y^2} + \frac{\partial^2\Phi}{\partial z^2} = 0. \tag{13}$$

In the present case the wing is slender of high-aspect ratio AR, thin and mildly cambered. This allows the wing to be modelled as an infinitesimally-thin flat lifting surface S_{wi}, like sketched in Fig. 5 (left). The wake is attached to the trailing edge (TE) as the time-dependent wavy surface S_{wa}. For small-amplitude motion the lifting surface and its time-dependent wake are projected on the plane $z = 0$, where linearized boundary conditions are imposed, e.g., [22]. The wing reference surface $S_{wi} + S_{wa}$, i.e., $x \in [0, c], y \in [-b/2, b/2]$ carries a dipole distribution $\mu(x, y, t)$ with the edge conditions $\mu(x = 0, y, t) = 0$ and $\mu(x, \pm b/2, t) = 0$. The wake reference surface $x \in [c, \infty], y \in [-b/2, b/2]$ also carries a dipole distribution $\mu(x, y, t)$ with the edge condition $\mu(x, \pm b/2, t) = 0$ and along the connection between wing and wake the continuity condition $\mu(c^-, y, t) = \mu(c^+, y, t)$. Along the edge far downstream $\mu(x = \infty, y, t) \neq 0$, except for $y = \pm b/2$, which corresponds to the vortex filament that formed at the very start of the motion of the wing, at $t = 0^+$.

The dipole distribution $\mu(x, y, t)$, a scalar quantity, is equivalent to a vortex distribution $\vec{\gamma}(x, y, t)$, a surface-vector quantity, through the relation:

$$\vec{\gamma}(x, y, t) = \vec{e}_n \times \vec{\nabla}\mu, \tag{14}$$

Eq. (14) implies that the surface vector $\vec{\gamma}$ is tangential to the plane $z = 0$ and is simultaneously normal to the gradient $\vec{\nabla}\mu$ of the dipole distribution on this plane. The vector $\vec{\nabla}\mu$ is a surface-vector perpendicular to the iso-contours of the dipole distribution. Vortex lines, similar to streamlines, are defined as curves everywhere tangential to $\vec{\gamma}$, so that Eq. (14) implies that vortex lines coincide with iso-dipole contours on the plane $z = 0$. So, conveniently, an iso-dipole plot on the surface $z = 0$ is equivalent to a plot of vortex lines on the plane $z = 0$.

A discontinuity in the dipole distribution along some curve on the surface $z = 0$, corresponds to a vortex filament along this curve, with the strength of the vortex filament equal to the local value of the discontinuity in the dipole distribution. The formulation in terms of the dipole distribution intrinsically obeys Kelvin-Helmholtz's vortex laws. Specifically, any vortex line on $S(x, y, t)$ is either a closed curve in itself, or a curve on $S(x, y, t)$ that feeds into a vortex filament and subsequently emerges from the vortex filament in order to form a closed vortex line.

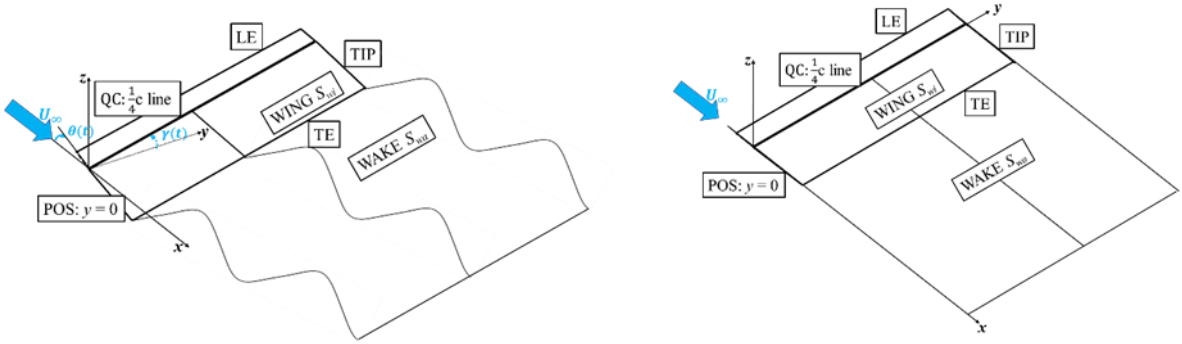

Fig. 5 Starboard side flapping-wing configuration at certain instant in cycle. Left: Flapping-pitching thin wing with wavy wake. Right: Stationary reference surface for application unsteady transpiration boundary conditions on wing and wake. Note that origin is on quarter-chord line QC.

The velocity potential $\Phi(\vec{x}, t)$, at time t at point $\vec{x}$, is split in the contribution $U_\infty x$ due to the uniform free stream and a (perturbation) velocity potential $\varphi_d(\vec{x}, t)$ due to the dipole distribution on $S_{wi} + S_{wa}$, i.e.,

$$\Phi(\vec{x}, t) = U_\infty x + \varphi_d(\vec{x}, t), \text{ with } \varphi_d(|\vec{x}| \to \infty, t) \to 0. \tag{15}$$

The velocity potential $\varphi_d(\vec{x}_0, t)$ induced at $\vec{x}_0$, at time t, by the dipole distribution $\mu(\vec{x}, t)$, on the surface $S_{wi} + S_{wa}$, is obtained from the surface integral:

$$\varphi_d(\vec{x}_0, t) = \frac{1}{4\pi} \iint_{S_{wi}+S_{wa}} \mu(\vec{x}, t) \frac{\vec{e}_n \cdot (\vec{x}_0 - \vec{x})}{|\vec{x}_0 - \vec{x}|^3} dS(\vec{x}), \tag{16}$$

with $\vec{x} = x\vec{e}_x + y\vec{e}_y$. In Eq. (16) $\vec{e}_n = \vec{e}_z$ is the unit vector perpendicular to the surface $S_{wi} + S_{wa}$, i.e., the plane $z = 0$, $\mu(\vec{x}, t) = \mu(x, y, t)$ and $dS(\vec{x}) = dxdy$.

The velocity $\vec{u}_d(\vec{x}_0, t) = \vec{\nabla}\varphi_d(\vec{x}_0, t)$, induced by the dipole distribution $\mu(x, y, t)$ on $S_{wi} + S_{wa}$, follows from taking the derivative of Eq. (16) with respect to $\vec{x}_0$. The derivation of obtaining $\vec{\nabla}\varphi_d(\vec{x}_0, t)$ is given amongst others in Ref. 22. It yields:

$$\vec{u}_d(\vec{x}_0, t) = \frac{1}{4\pi} \iint_{S_{wi}+S_{wa}} \frac{\vec{\gamma}(x,y,t) \times (\vec{x}_0 - \vec{x})}{|\vec{x}_0 - \vec{x}|^3} dxdy - \frac{1}{4\pi} \int_{\partial(S_{wi}+S_{wa})} \mu(x, y, t) \frac{(\vec{x}_0 - \vec{x}) \times \vec{dl}(\vec{x})}{|\vec{x}_0 - \vec{x}|^3}, \tag{17}$$

with, in the first term $\vec{\gamma}(x, y, t) = \vec{e}_z \times \vec{\nabla}\mu$, given in Eq. (14), the vortex distribution on the surface carrying the dipole distribution $\mu(x, y, t)$. The reference surface representing the wing and its wake, i.e., $S_{wi} + S_{wa}$, forms a vortex sheet in 3D space. The second term in Eq. (17) is recognised as the law of Biot and Savart for the velocity induced by a vortex filament in 3D space. In this case the vortex filament is along the boundary (i.e., the closed edge $\partial(S_{wi} + S_{wa})$ of the reference surface of the wing and its wake. The strength of the vortex filament equals the local strength $\mu(\vec{x} \in \partial(S_{wi} + S_{wa}), t)$ of the dipole distribution, while $\vec{dl}(\vec{x})$ is an infinitesimal element of the vortex filament.

The surface integrals in Eqs. (16) and (17) are singular integrals, i.e., when $\vec{x}_0 \to \vec{x} = x\vec{e}_x + y\vec{e}_y$, a point on the dipole/vortex sheet $S_{wi} + S_{wa}$, the integrand of the surface integrals tend to infinity. However, the result of the evaluation of these integrals, i.e., the velocity potential and the velocity, is finite, though discontinuous. To obtain this result, the integrals are evaluated as Cauchy-Principle-Value (CPV) integrals [22].

For $\vec{x}_0 \in \partial(S_{wi} + S_{wa})$, the second term in Eq. (17) for the induced velocity due to the vortex filament, is singular, like $1/r$, with $r \to 0$ the distance from the filament. For a curved vortex filament there is an additional singular term that behaves like $\ln r$. In the present investigation both these terms are omitted from the induced velocity, or, rather avoided by limiting the distance to the filament to a certain cut-off value.

The result of this CPV procedure for the velocity potential, $\varphi_d(\vec{x}_0, t)$ is that for $\vec{x}_0 \in S_{wi+wa}(x, y)$:

$$\varphi_d(\vec{x}_0, t) = \pm\frac{1}{2}\mu(x_0, y_0, t) + \frac{1}{4\pi}\text{CPV} \iint_{S_{wi}+S_{wa}} \mu(x, y, t) \frac{\vec{e}_z \cdot (\vec{x}_0 - \vec{x})}{|\vec{x}_0 - \vec{x}|^3} dxdy \tag{18}$$

and for the induced velocity $\vec{u}_d(\vec{x}_0, t)$:

$$\vec{u}_d(\vec{x}_0,t) = \pm\frac{1}{2}\vec{\gamma}(x_0,y_0,t)\times\vec{e}_z + \frac{1}{4\pi}\mathrm{CPV}\iint_{S_{wi}+S_{wa}}\frac{\vec{\gamma}(x,y,t)\times(\vec{x}_0-\vec{x})}{|\vec{x}_0-\vec{x}|^3}dxdy - \frac{1}{4\pi}\int_{\partial(S_{wi}+S_{wa})}\mu(x,y,t)\frac{(\vec{x}_0-\vec{x})\times\vec{dl}(\vec{x})}{|\vec{x}_0-\vec{x}|^3}, \quad (19)$$

with $\vec{\gamma}\times\vec{e}_z = \vec{\nabla}\mu = \frac{\partial\mu}{\partial x}\vec{e}_x + \frac{\partial\mu}{\partial y}\vec{e}_y$. In Eqs. (18) and (19) the $\pm$ symbol indicates that the quantity is positive on the upper side of $S_{wi+wa}(x,y)$ and negative on the lower side of $S_{wi+wa}(x,y)$.

B. Bernoulli's Equation

The momentum equation for inviscid, incompressible, irrotational flow, not subjected to a body force field, like gravity, reads:

$$\frac{\partial\vec{u}}{\partial t} + \vec{\nabla}\frac{1}{2}|\vec{u}|^2 + \vec{\nabla}\frac{p}{\rho_\infty} = \vec{0}. \quad (20)$$

Employing $\vec{u} = \vec{\nabla}\Phi$, upon integration with respect to space, then results in Bernoulli's equation for inviscid, incompressible, irrotational flow, not subjected to body forces, i.e.,

$$\frac{\partial\Phi}{\partial t} + \frac{1}{2}\left|\vec{\nabla}\Phi\right|^2 + \frac{p}{\rho_\infty} = C(t), \quad (21)$$

with $C(t)$ independent of position in space, so, either a constant, or a function of time in the whole space. In the present case, the constant is evaluated in the far-field, which yields $C(t) = C = \frac{1}{2}U_\infty^2 + \frac{p_\infty}{\rho_\infty}$, so that with $\Phi(\vec{x},t) = U_\infty x + \varphi_d(\vec{x},t)$, $\vec{\nabla}\Phi(\vec{x},t) = U_\infty\vec{e}_x + \vec{u}_d(\vec{x},t)$ and the pressure coefficient $C_p(\vec{x},t)$ defined as

$$C_p(\vec{x},t) \equiv \frac{p(\vec{x},t)-p_\infty}{\frac{1}{2}\rho_\infty U_\infty^2}, \quad (22)$$

$$C_p(\vec{x},t) = -\frac{2}{U_\infty^2}\frac{\partial\varphi_d}{\partial t} - [2\frac{\vec{e}_x.\vec{u}_d}{U_\infty} + \frac{|\vec{u}_d|^2}{U_\infty^2}]. \quad (23)$$

For points on the wing and on the wake in the plane $z = 0$, it follows

$$C_p(x,y,t) = -\frac{2}{U_\infty^2}\frac{\partial\varphi_d}{\partial t} - \frac{2}{U_\infty}u_d(x,y,t) - \frac{2}{U_\infty^2}|\vec{u}_d(x,y,t)|^2. \quad (24)$$

In this expression, the first two terms are linear, while the third term is quadratic, which is neglected in the linearized formulation.

C. Boundary Conditions

In order to solve for the dipole distribution $\mu(x,y,t)$ on the wing S_{wi}, the boundary condition is the normal-velocity condition, i.e., the no-penetration condition, given by

$$(\vec{u} - \vec{u}_{wi}).\vec{e}_n = 0, \text{ for points on } S_{wi}, \quad (25)$$

which assures that, in normal direction, the wing surface moves at the same speed as the flow. In order to impose this condition, it has to be converted into a transpiration condition to be applied at the reference surface S_{wi}. In the present study, in which a lifting-line method has been developed, this is not needed, there are no explicit boundary conditions imposed on S_{wi}.

On the wake surface S_{wa}, both the dipole distribution $\mu(x,y,t)$ and the location of the wake surface S_{wa} are to be solved for. Therefore, two boundary conditions have to be imposed: the normal-velocity boundary condition, Eq. (25) and the condition that the wake surface does not carry a load, i.e., that the pressure difference across the wake surface equals zero. Using Eq. (24), the latter condition, applied at S_{wa}, yields:

$$\Delta C_p(x,y,t) = -\frac{2}{U_\infty^2}\frac{\partial\Delta\varphi_d}{\partial t} - \frac{2}{U_\infty}\Delta u_d(x,y,t) - \frac{2}{U_\infty^2}\Delta[|\vec{u}_d(x,y,t)|^2], \text{ for points on } S_{wa}. \quad (26)$$

D. Prandtl's Lifting-Line Method

The lifting-line theory of Prandtl for high-aspect-ratio wings in **steady**, incompressible, irrotational (potential) flow, can be formulated in terms of the dipole/vortex-distribution described in section IV.A, see Fig. 5 (right). From Eq. (14) it follows that, on the reference surface $z = 0$ of the wing and its wake, the vortex distribution $\vec{\gamma}(x,y)$ can be expressed in terms of the partial derivatives, with respect to x and y, of the dipole distribution $\mu(x,y)$ as:

$$\vec{\gamma}(x,y) = \vec{e}_z\times\vec{\nabla}\mu = -\frac{\partial\mu}{\partial y}\vec{e}_x + \frac{\partial\mu}{\partial x}\vec{e}_y. \quad (27)$$

The spanwise component $\gamma_y(x,y)$ of the wing vortex distribution is lumped into the spanwise distribution of the section circulation $\Gamma(y)$ of the wing, through

$$\Gamma(y) \equiv \int_0^c \gamma_y(x,y)dx = \int_0^c \frac{\partial\mu}{\partial x}dx = \mu(c,y), \text{ for } y\in[-b/2,b/2], \quad (28)$$

where the (leading-)edge condition $\mu(0, y) = 0$ has been imposed. For each section $y =$ constant of the wing, the circulation $\Gamma(y)$ is positioned at the center-of-vorticity (COV) of the spanwise component of the vortex distribution $\gamma_y(x, y)$, with

$$x_{COV}(y)\Gamma(y) \equiv \int_0^c x\gamma_y(x, y)dx. \tag{29}$$

Prandtl placed the circulation at the quarter-chord line of the wing, therefore here the spanwise distribution of the circulation of the wing is denoted as $\Gamma(y) = \Gamma_{c/4}(y)$. Prandtl's choice can be related to the classical complex-function solution of the incompressible 2D potential flow about a flat plate at angle of attack, e.g. [25]. Alternatively, it can be related to Prandtl's thin-airfoil solution for incompressible 2D potential flow about thin airfoils at angle of attack, e.g. [26]. From these solutions it follows $\gamma_y(x) = A\sqrt{(c - x)/x}$, with the constant A proportional to the free stream velocity U_∞ and the angle of attack.

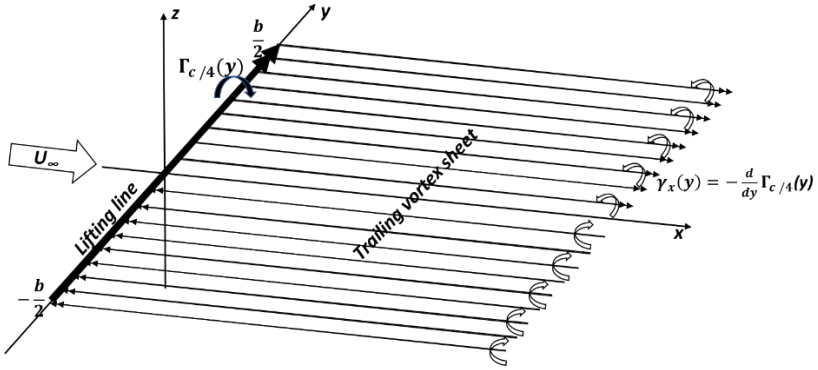

Fig. 6 Prandtl's lifting-line method for incompressible potential flow about high-aspect ratio wing at angle of attack. Note that origin coordinate system is on lifting line.

Substitution of this solution in Eq. (29) leads to $x_{COV} = c/4$. The dipole distribution on the wing and wake in Fig. 5 (right) is now, see Fig. 6:

$$\mu(x, y) = \Gamma_{c/4}(y), \text{ for } x \in [0, \infty) \text{ and } y \in [-b/2, b/2], \tag{30}$$

equivalent to a spanwise vortex filament of strength $\Gamma_{\frac{c}{4}}(y)$, with $\Gamma_{c/4}(\pm b/2) = 0$, and a continuous distribution of the chordwise component $\gamma_x(y) = -\frac{d}{dy}\Gamma_{c/4}(y)$ of the vortex distribution on the region downstream of the lifting line. Finally, formally, there is also a vortex filament of strength $-\Gamma_{c/4}(y)$ along the line $x = \infty$, $z = 0$, for $y \in [-b/2, b/2]$, the so-called start vortex, but its induced velocity at the lifting line is negligibly small. Note that a vortex line starting in the lifting-line running in spanwise direction, emerges at some point along the span, turns abruptly in chordwise direction, continues straight on until at infinity downstream it meets the start vortex filament. There it turns abruptly in negative *y*-direction and runs chordwise upstream, until it meets the lifting-line vortex filament, where it turns abruptly in positive *y*-direction until it arrives at its initial point, completing the closed circuit, obeying the Kelvin-Helmholtz vortex laws.

In Prandtl's lifting-line method the distribution of the circulation $\Gamma_{c/4}(y)$ along the lifting line is obtained from an integro-differential equation that evolves from an intricate combination of the relation for sectional lift $\ell(y)$ [N/m], obtained from the Kutta-Joukowski Theorem for the force on a vortex filament and the expression for the sectional lift in terms of the slope $a_0 = 2\pi$ of the sectional lift vs angle-of-attack curve, obtained from thin-airfoil theory.

The Kutta-Joukowski Theorem, provides the sectional lift $\ell(y)$ in terms of the circulation $\Gamma_{c/4}(y)$ of the wing, the free-stream velocity U_∞ and the density ρ_∞, as

$$\ell(y) = \rho_\infty U_\infty \Gamma_{c/4}(y). \tag{31}$$

Thin-airfoil theory gives the lift coefficient $c_\ell(y)$ in terms of the slope $\frac{d}{d\alpha}c_\ell(y) = a_0(y)$ of the lift curve $c_\ell(\alpha)$, the dynamic pressure $q_\infty = \frac{1}{2}\rho_\infty U_\infty^2$, the chord $c(y)$ of the airfoil section and the effective angle of attack of the airfoil section:

$$\ell(y) \equiv \tfrac{1}{2}\rho_\infty U_\infty^2 c_\ell(y)c(y), \tag{32}$$

with the lift coefficient $c_\ell(y)$ expressed as

$$c_\ell(y) = a_0(y)(\alpha - \alpha_0(y) + \beta(y) + \tfrac{w_{in}(y)}{U_\infty}), \tag{33}$$

with α the geometric angle of attack of the wing, $\alpha_0(y)$ the zero-lift angle of attack of the airfoil section at the spanwise section y considered, $\beta(y)$ the spanwise distribution of the twist angle of the wing, with at the root of the wing $\beta(0) = 0$ and finally, $w_{in}(y)$ the z-component of the velocity induced at the lifting line by the trailing vortex sheet. Combining Eqs. (31)-(33) yields

$$\Gamma_{\frac{c}{4}}(y) = \frac{1}{2}U_\infty c(y)a_0(y)[\alpha - \alpha_0(y) + \beta(y) + \frac{w_{in}(y)}{U_\infty}], \text{ for } y \in [-b/2, b/2] \quad (34)$$

The upwash $w_{in}(y)$, induced by the chordwise vortex distribution $\gamma_x(y) = -\frac{d}{dy}\Gamma_{c/4}(y)$ on the trailing vortex sheet, $(x \in [0,\infty), y \in [-b/2, b/2], z = 0)$, see Fig. 6, follows from Eq. (19) as

$$w_d(x_0, y_0, z_0 = 0) = \frac{1}{4\pi}\text{CPV}\int_{-b/2}^{b/2}\left[-(y_0 - y)\frac{d}{dy}\Gamma_{c/4}(y)\int_0^\infty \frac{dx}{[(x_0-x)^2+(y_0-y)^2]^{3/2}}\right]dy$$

The integral with respect to x can be evaluated analytically, which leads to

$$w_d(x_0, y_0, z_0 = 0) = \frac{-1}{4\pi}\text{CPV}\int_{-b/2}^{b/2}\frac{1}{y_0-y}\frac{d}{dy}\Gamma_{c/4}(y)\left[1 + \frac{x_0}{[x_0^2+(y_0-y)^2]^{1/2}}\right]dy.$$

The upwash to be substituted in Eq. (34) equals $w_{in}(y_0) = w_d(x_0 = 0, y_0, z_0 = 0)$, so that

$$w_{in}(y) = \frac{-1}{4\pi}\text{CPV}\int_{-b/2}^{b/2}\frac{1}{y-\eta}\frac{d}{d\eta}\Gamma_{c/4}(\eta)d\eta.$$

Substitution in Eq. (34) yields Prandtl's integro-differential equation for the unknown spanwise distribution of the section circulation $\Gamma_{c/4}(y)$:

$$\Gamma_{c/4}(y) = \frac{1}{2}U_\infty c(y)a_0(y)[\alpha - \alpha_0(y) + \beta(y) - \frac{1}{4\pi U_\infty}\text{CPV}\int_{-\frac{b}{2}}^{\frac{b}{2}}\frac{1}{y-\eta}\frac{d}{d\eta}\Gamma_{c/4}(\eta)d\eta], \text{ for } y \in [-b/2, b/2]. \quad (35)$$

E. Kutta-Joukowski Theorem for Unsteady Flow

The flow about a flapping wing is an unsteady flow problem. In the case of **unsteady**, incompressible, potential flow, Laplace's equation, Eq. (13), is the governing equation for the velocity potential, like for steady, incompressible, potential flow. The unsteadiness enters the problem through the boundary conditions, i.e., the motion of the wing. Furthermore, as a consequence of the temporal variation of the circulation, the wake is now a vortex sheet of strength depending on the history of the circulation of the wing, i.e., of the history of the motion of the wing.

For unsteady flow, Eq. (31) has to be adjusted since the classical Kutta-Joukowski Theorem is for steady flow only. For unsteady potential flow, Eq (24) for the pressure coefficient $C_p(x, y, t)$ has been derived from the momentum equation for unsteady, incompressible potential flow. From Eq. (24) the pressure jump across the wing reference surface S_{wi} is derived, to first order in the perturbations, as:

$$\Delta C_p(x, y, t) \equiv \frac{p(x,y,z=0^-)-p(x,y,z=0^+)}{\frac{1}{2}\rho_\infty U_\infty^2} = \frac{2}{U_\infty}\left[\frac{\partial\Delta\varphi}{\partial x} + \frac{1}{U_\infty}\frac{\partial\Delta\varphi}{\partial t}\right] + h.o.t.,$$

(36)

with $\varphi(x, y, z, t)$ the perturbation velocity potential and $\Delta\varphi \equiv \varphi(x, y, z = 0^+) - \varphi(x, y, z = 0^-)$. In the present formulation the reference surface $S_{wi} + S_{wa}$ of the wing and the wake, carry a dipole distribution $\mu(x, y, t)$, so that the jump in the perturbation potential can be expressed as $\Delta\varphi(x, y, 0, t) = \mu(x, y, t)$. Then Eq. (36) becomes

$$\Delta C_p(x, y, 0, t) = \frac{2}{U_\infty}\left[\frac{\partial\mu}{\partial x} + \frac{1}{U_\infty}\frac{\partial\mu}{\partial t}\right] \quad (37)$$

To derive an expression for the Kutta-Joukowski Theorem for unsteady flow about thin wings, the pressure difference, given in Eq. (37), is integrated along the section of the wing reference surface, situated in the plane $z = 0$, i.e.,

$$\frac{\ell(y,t)}{\frac{1}{2}\rho_\infty U_\infty^2 c(y)} = \frac{1}{c(y)}\int_0^{c(y)}\Delta C_p(x, y, t)dx = \frac{2}{c(y)U_\infty}\int_0^{c(y)}[\frac{\partial\mu}{\partial x} + \frac{1}{U_\infty}\frac{\partial\mu}{\partial t}]dx. \quad (38)$$

Since, $\int_0^{c(y)}\frac{\partial\mu}{\partial x}(x, y, t)dx = \mu(c(y), y, t) = \int_0^{c(y)}\gamma_y(x, y, t)dx = \Gamma(y, t)$, it follows:

$$\frac{\ell(y,t)}{\frac{1}{2}\rho_\infty U_\infty^2 c(y)} = \frac{2}{c(y)U_\infty}[\Gamma(y, t) + \frac{1}{U_\infty}\frac{\partial}{\partial t}\int_0^{c(y)}\mu(x, y, t)dx] \quad (39)$$

Consider the remaining integral in Eq. (39). Partial integration gives, with $\frac{\partial\mu}{\partial x} = \gamma_y$:

$$\int_0^{c(y)}\mu(x, y, t)dx = [\mu(x, y, t)x]|_0^{c(y)} - \int_0^{c(y)}x\frac{\partial}{\partial x}\mu(x, y, t)dx = \Gamma(y, t)c(y) - \int_0^{c(y)}x\gamma_y(x, y, t)dx.$$

Therefore, with the definition of the center-of-gravity of the spanwise component of the vortex distribution, defined in Eq. (29), Eq. (39) results in

$$\frac{\ell(y,t)}{\frac{1}{2}\rho_\infty U_\infty^2 c(y)} = \frac{2}{c(y)U_\infty}[\Gamma(y, t) + \frac{1}{U_\infty}\frac{\partial}{\partial t}\{\Gamma(y, t)c(y)\left\{1 - \frac{x_{\text{COV}}(y,t)}{c(y)}\right\}\}] \quad (40)$$

Similar to the argumentation following Eq. (29), it is assumed that $\frac{x_{\text{COV}}(y,t)}{c(y)} \approx \frac{1}{4}$. Then it follows

$\frac{\ell(y,t)}{\frac{1}{2}\rho_\infty U_\infty^2 c(y)} = \frac{2}{c(y)U_\infty}[\Gamma(y,t) + \frac{3}{4}\frac{c(y)}{U_\infty}\frac{\partial}{\partial t}\Gamma(y,t)]$,

so that the Kutta-Joukowski Theorem for unsteady flow reads:

$$l(y,t) = \rho_\infty U_\infty \left[\Gamma(y,t) + \frac{3}{4}\frac{c(y)}{U_\infty}\frac{\partial}{\partial t}\Gamma(y,t)\right]. \quad (41)$$

In Eq. (41) the first term is the conventional term for the lift due to the circulation of the airfoil section, while the second term is the contribution to the lift of the added-mass effect induced by the motion of the wing section.

The relation presented in Eq. (41) is different from the relation for the section lift coefficient as for example given in [27], which instead of the factor $\frac{3}{4}$ features the factor 1.0 in the added-mass contribution to the section lift.

F. Lifting-Line Method for Unsteady Flow

For the case of steady flow, the lifting-line integro-differential equation follows from the combination of Eqs. (31), (32) and (33). For unsteady flow, the classical Kutta-Joukowski Theorem Eq. (31), is replaced by its unsteady variant. Then Eq. (34) becomes

$$\Gamma_{c/4}(y,t) + \frac{3}{4}\frac{c(y)}{U_\infty}\frac{\partial}{\partial t}\Gamma_{c/4}(y,t) = \frac{1}{2}U_\infty c(y) a_0(y)[\alpha_{eff}(y,t) - \alpha_0(y) + \beta(y) + \frac{w_{in}(y,t)}{U_\infty}], \quad (42)$$

for $y \in [-b/2, b/2]$ and $t > 0$.

In Eq. (42) the upwash $w_{in}(y,t)$ due to the dipole distribution on the wing between the lifting line at $x = c(y)/4$ and the trailing edge $x = x_{TE}^- = c(y)$, together with the dipole distribution on on the wake, which runs from $x = x_{TE}^+ = c(y)$, to infinity downstream, see Fig. 5-right, equals

$$w_{in}(y,t) = \frac{1}{4\pi}\int_{-\frac{b}{2}}^{\frac{b}{2}} d\eta \left[\int_{c(y)/4}^{c(y)} \frac{(y-\eta)\gamma_x(\eta,t)}{[x^2+(y-\eta)^2]^{\frac{3}{2}}} dx + \int_{c(y)}^{\infty} \frac{(y-\eta)\gamma_x(x,\eta,t) + x\gamma_y(x,\eta,t)}{[x^2+(y-\eta)^2]^{\frac{3}{2}}} dx\right], \text{ for } y \in [-b/2, b/2]. \quad (43)$$

Note that between the lifting line at $x = c/4$ and the trailing edge at $x = c$, the wing reference surface carries a dipole distribution $\mu(x,y,t) = \Gamma_{c/4}(y,t)$, which corresponds to a vortex distribution with a chordwise component $\gamma_x(y,t)$ only.

Equation (43) is an integro-differential equation for $\Gamma_{c/4}(y,t)$. However, now the situation is more complicated than for the case of steady flow in that the strength (circulation) $\Gamma_{c/4}(y,t)$ of the lifting line is time-dependent, while the wake carries a dipole distribution $\mu(x,y,t)$ that depends not only on *y*, but on *x*, *y* and *t*, so that for the wake the contribution from both components of the vortex distribution, i.e., $\gamma_x = -\frac{\partial \mu}{\partial y}$ and $\gamma_y = \frac{\partial \mu}{\partial x}$, have to be considered.

G. Boundary Conditions on Wake

The wake is subject to two boundary conditions, see section IV.B. In the present study, the condition that the wake surface should be a stream surface, Eq. (25), is omitted since the true wake surface is not part of the formulation, i.e., just the wake reference surface $z = 0$ is considered. Note that once the dipole distribution has been determined, the planar wake reference surface features a distribution of non-zero normal velocity that might be used to update the geometry of the wake surface in an iterative manner.

The second condition, Eq. (26), that across the wake the jump in pressure ΔC_p equals zero, is employed to determine the spatial and temporal strength of the wake dipole distribution. Equation (37) applied to the wake reference surface reads:

$$\Delta C_p(x > x_{TE}, y, t) = \frac{2}{U_\infty}\left[\frac{\partial \mu}{\partial x} + \frac{1}{U_\infty}\frac{\partial \mu}{\partial t}\right] = 0, \text{ for } y \in [-b/2, b/2] \text{ and } t > 0. \quad (44)$$

Eq. (44) is recognized as a first-order wave equation in (*x*,*t*)-space, for $\mu(x,y,t)$ convecting with constant velocity U_∞ in *x*-direction. Then it follows that at time *t* the solution $\mu(x,y,t)$ equals:

$$\mu(x,y,t) = \Gamma_{c/4}\left(y, t - \frac{x - x_{TE}}{U_\infty}\right), \text{ for } x \in [x_{TE}^+, x_{TE}^+ + U_\infty t],\ y \in [-b/2, b/2] \text{ and } t > 0. \quad (45)$$

The classical Lifting-Line method does not require a Kutta condition at the trailing edge: Actually, in its problem formulation does not feature the solid part of the wing nor the trailing edge. For the unsteady-flow version of the lifting-line method there is a trailing edge, at $x = c$, which forms the connection between the wing and the wake. This implies that a Kutta condition is to be imposed. The condition is that at the trailing edge, the pressure difference between upper and lower side of the surface equals zero at all times. This implies that the linearized equation given in Eq. (44) is not only applied on the wake surface, but also at the trailing edge of the wing. Therefore, the Kutta condition for unsteady flow reads:

$$\Delta C_p(x = x_{TE}^- = c, y, t) = \frac{2}{U_\infty}\left[\frac{\partial \mu}{\partial x} + \frac{1}{U_\infty}\frac{\partial \mu}{\partial t}\right] = 0, \text{ i.e., } \frac{\partial \mu}{\partial x} + \frac{1}{U_\infty}\frac{\partial \mu}{\partial t} = 0, \quad (46)$$

for $x = x_{TE}^{-} = c, z = 0$, along the span of the trailing edge, for all times.

H. Spanwise Distributions Section Lift, Drag and Pitching Moment

The spanwise distribution of the section lift $\ell(y,t)$ is given in Eq. (41), repeated here, in terms of the unsteady Kutta-Joukowski Theorem.

$$l(y,t) = \rho_\infty U_\infty \left[\Gamma_{c/4}(y,t) + \tfrac{3}{4}\tfrac{c(y)}{U_\infty}\tfrac{\partial}{\partial t}\Gamma_{c/4}(y,t)\right]. \tag{41}$$

The section drag $d(y,t)$ follows from application of the Kutta-Joukowski Theorem to the lifting-line vortex filament subject to an upwash velocity component:

$$d(y,t) = -\rho_\infty U_\infty \left[\tfrac{w_{in}(y,t)}{U_\infty} - \tfrac{1}{U_\infty}\tfrac{\partial h(y,t)}{\partial t}\right]\Gamma_{c/4}(y,t) \tag{47}$$

The term inside the square brackets is the velocity in *z*-direction, relative to the flapping motion of the lifting line, consisting of the contribution induced by the dipole distribution on the wing and on the wake, with the upwash corrected for the time-derivative of the position of the lifting line. Once the circulation distribution of the lifting-line has been determined from the Unsteady-Lifting-Line integro-differential equation, Eq. (42), the velocity induced at the lifting line by the dipole distribution follows as

$$\tfrac{w_{in}(y,t)}{U_\infty} = \tfrac{2}{a_0(y)}\tfrac{\bar{c}}{c(y)}\tfrac{1}{U_\infty \bar{c}}\left[\Gamma_{c/4}(y,t) + \tfrac{3}{4}\tfrac{c(y)}{U_\infty}\tfrac{\partial}{\partial t}\Gamma_{c/4}(y,t)\right] - [\alpha_{eff}(y,t) - \alpha_0(y) + \beta(y)] \tag{48}$$

Equation (4) gives the effective angle of attack $\alpha_{eff}(y,t)$ as the sum of the pitch angle $\theta(t)$ and the plunge angle $-\tfrac{1}{U_\infty}\tfrac{\partial h(y,t)}{\partial t}$. Substitution in Eq. (47) yields:

$$d(y,t) = -\rho_\infty U_\infty \Gamma_{c/4}(y,t)\left[\tfrac{2}{a_0(y)}\tfrac{\bar{c}}{c(y)}\tfrac{1}{U_\infty \bar{c}}\left\{\Gamma_{c/4}(y,t) + \tfrac{3}{4}\tfrac{c(y)}{U_\infty}\tfrac{\partial}{\partial t}\Gamma_{c/4}(y,t)\right\} - \{\theta(t) - \alpha_0(y) + \beta(y)\}\right] \tag{49}$$

The section lift coefficient $c_l(y,t)$ and section drag coefficient $c_d(y,t)$ then follow by dividing left- and right-hand side of Eqs. (41) and (49), respectively, by $\tfrac{1}{2}\rho_\infty U_\infty^2 c(y)$, i.e.:

$$c_\ell(y,t) = 2\left[\tfrac{\bar{c}}{c(y)}\tfrac{\Gamma_{c/4}(y,t)}{U_\infty \bar{c}} + \tfrac{3}{4}\tfrac{\bar{c}}{U_\infty}\tfrac{\partial}{\partial t}\tfrac{\Gamma_{c/4}(y,t)}{U_\infty \bar{c}}\right] \text{ and } c_d(y,t) = -2\tfrac{\bar{c}}{c(y)}\left[\tfrac{w_{in}(y,t)}{U_\infty} - \tfrac{1}{U_\infty}\tfrac{\partial}{\partial t}h(y,t)\right]\tfrac{\Gamma_{c/4}(y,t)}{U_\infty \bar{c}}. \tag{50}$$

The section pitching moment $c_m(y,t)$, around the quarter-chord line $x = x_{\frac{c}{4}}$, z = 0, is defined as:

$$m(y,t) = -\tfrac{1}{2}\rho_\infty U_\infty^2 \int_0^c \Delta C_p(x,y,0,t)(x - x_{\frac{c}{4}})\,dx, \text{ positive clockwise,} \tag{51a}$$

with $\Delta C_p(x,y,0,t)$ given in Eq. (37). Then the section pitching moment coefficient equals

$$c_m(y,t) \equiv \tfrac{m(y,t)}{\frac{1}{2}\rho_\infty U_\infty^2 c(y)^2} = -\tfrac{1}{c(y)^2}\int_0^c \Delta C_p(x,y,0,t)(x - x_{\frac{c}{4}})\,dx. \tag{51b}$$

Substitution of Eq. (37) yields

$$\begin{aligned} c_m(y,t) &= -\tfrac{2}{U_\infty c(y)^2}\int_0^c \left(x - x_{\frac{c}{4}}\right)\tfrac{\partial \mu}{\partial x}dx - \tfrac{2}{U_\infty^2 c(y)^2}\tfrac{\partial}{\partial t}\int_0^c \left(x - x_{\frac{c}{4}}\right)\mu dx \\ &= -\tfrac{2}{U_\infty c(y)^2}[i_1(y,t) - x_{\frac{c}{4}} i_0(y,t)] - \tfrac{2}{U_\infty^2 c(y)^2}\tfrac{\partial}{\partial t}[j_1(y,t) - x_{\frac{c}{4}} j_0(y,t)] \end{aligned} \tag{51c}$$

The four integrals are evaluated as:

$$i_0(y,t) = \int_0^c \tfrac{\partial \mu}{\partial x}dx = [\mu(x,y,t)]|_0^c = \Gamma(y,t),$$

since at the leading edge $\mu(x = 0, y, t) = 0$, while at the trailing edge: $\mu(x = c, y, t) = \Gamma(y,t)$.

$$i_1(y,t) = \int_0^c \tfrac{\partial \mu}{\partial x}x dx = \int_0^c \gamma_y(x,y,t)\,x dx = \Gamma(y,t)x_{COV},$$

with the "center-of-vorticity" (COV), defined in Eq. (29).

$$\begin{aligned} j_0(y,t) &= \int_0^c \mu(x,y,t)\,dx = [(x\mu(x,y,t)]|_0^c - \int_0^c \tfrac{\partial \mu}{\partial x}(x,y,t)\,x dx \\ &= c\Gamma(y,t) - x_{COV}\Gamma(y,t) = (c - x_{COV})\Gamma(y,t). \end{aligned}$$

Finally,

$$\begin{aligned} j_1(y,t) &= \int_0^c \mu(x,y,t)\,x dx = \left[(\tfrac{1}{2}x^2\mu(x,y,t)\right]\Big|_0^c - \tfrac{1}{2}\int_0^c \tfrac{\partial \mu}{\partial x}(x,y,t)\,x^2 dx \\ &= \tfrac{1}{2}c^2\Gamma(y,t) - \tfrac{1}{2}x_{COV2}^2\Gamma(y,t), \end{aligned}$$

with the second moment of the spanwise component of the vortex distribution $\gamma_y(x,y,t)$, defined as:

$$x_{COV2}^2\Gamma(y,t) = \int_0^c \gamma_y(x,y,t)x^2\,dx. \tag{51d}$$

Substitution of the integrals in the expression for the section pitching moment, Eq. (50c), yields:

$$c_m(y,t) = -\tfrac{2}{U_\infty c(y)^2}(x_{COV} - x_{\frac{c}{4}})\Gamma(y,t) - \tfrac{2}{U_\infty^2 c(y)^2}\tfrac{\partial}{\partial t}[\Gamma(y,t)\{\tfrac{1}{2}(c^2 - x_{COV2}^2) - x_{\frac{c}{4}}(c - x_{COV})\}]. \tag{51e}$$

Assuming that the distribution of the spanwise component of the vortex distribution behaves like that of a thin airfoil, i.e., $\gamma_y(x) = A\sqrt{(c-x)/x}$, it follows $x_{COV2} = \frac{c}{4}\sqrt{2}$. So, with $x_{\frac{c}{4}} = \frac{c}{4}$ and $x_{COV} = \frac{c}{4}$, it follows

$$c_m(y,t) = -\frac{1}{2}\frac{1}{U_\infty^2}\frac{\partial}{\partial t}\Gamma(y,t) \tag{51f}$$

This shows that the section pitching moment is zero for steady flow, whereas for unsteady flow the pitch8ing moment is due to the added-mass term only.

I. Spanwise Distribution Power Required for Pitching and Flapping

The power required for flapping/pitching flight is the sum of the power required for pitching and the power required for flapping. The pitching motion $\theta(t)$ of the wing (sections), around the pitch axis (the quarter-chord line) is defined in Eq. (2). The flapping motion $\gamma(t)$, around the x-axis of the configuration, is defined in Eq. (1).

For pitching, the section power $p_p(y,t)$ required to rotate the wing section around the pitch axis, per unit length in spanwise direction, is minus the product of the section pitching moment $m(y,t)$ and the rate of pitching $\dot{\theta}(t)$, i.e.:

$$p_p(y,t) = -m(y,t)\frac{d\theta}{dt}, \tag{52a}$$

with $[p_p]$ = W/m, $[m]$ = Nm/m and θ in radians. In the form of the power coefficient $c_{p,p}(y,t)$, one obtains the contribution of pitching to the section power coefficient, as:

$$c_{p,p}(y,t) \equiv \frac{p_p(y,t)}{\frac{1}{2}\rho_\infty U_\infty^3 c(y)} = -\frac{m(y,t)}{\frac{1}{2}\rho_\infty U_\infty^2 c^2(y)}\frac{c(y)}{U_\infty}\frac{d\theta}{dt} = -c_m(y,t)\frac{c(y)}{U_\infty}\frac{d\theta}{dt}. \tag{52b}$$

For flapping, the section power $p_f(y,t)$ required to rotate the wing around the flap angle axis, per unit length in spanwise direction, is minus the product of the section lift $\ell(y,t)$, the lever $|y|$ and the rate of flapping $\dot{\gamma}(t)$, i.e.:

$$p_f(y,t) = -\ell(y,t)|y|\frac{d\gamma}{dt}, \tag{53a}$$

with $[p_f]$ = W/m, $[\ell]$ =N/m and γ in radians. In the form of the power coefficient $c_{p,f}(y,t)$, one obtains the contribution of flapping to the section power coefficient, as:

$$c_{p,f}(y,t) \equiv \frac{p_f(y,t)}{\frac{1}{2}\rho_\infty U_\infty^3 c(y)} = -\frac{\ell(y,t)}{\frac{1}{2}\rho_\infty U_\infty^2 c(y)}\frac{|y|}{b/2}\frac{b/2}{U_\infty}\frac{d\gamma}{dt} = -c_\ell(y,t)\frac{|y|}{b/2}\frac{b/2}{U_\infty}\frac{d\gamma}{dt}. \tag{53b}$$

IV. Application Unsteady Lifting-Line Method

A. Simplified Geometry Wing Robird

The spanwise distribution of the chord $c(y)$ of the Robird wing (Fig. 1) has been simplified to a piece-wise linear distribution, symmetric with respect to the plane-of-symmetry y = 0. The half-span is subdivided in three parts:

$y \in [0.0, 0.182]$ m : $c(y) = 0.2$ m
$y \in [0.182, 0.476]$ m: $c(y) = [0.200(0.476 - y) + 0.102(y - 0.182)]/0.294$ m
$y \in [0.476, 0.560]$ m: $c(y) = [0.102(0.560 - y) + 0.010(y - 0.476)]/0.084$ m

The distribution of the chord of the wing is shown in Fig. 7. The dimensions of the wing planform are provided in Table 1.

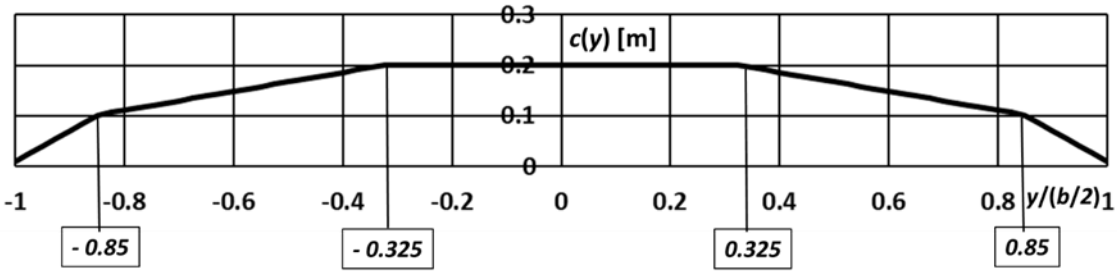

Fig. 7 Spanwise distribution of chord $c(y/0.5b)$ of simplified planform of wind-tunnel model Robird.

Table 1 Geometric parameters of simplified flapping-wing configuration.

b	1.12 m
c_0	0.2 m
$\bar{c}$	0.1527 m
AR	7.34

For reasons of convenience of modeling, the wing of the simplified configuration extends from the root of the wind-tunnel model to the plane of symmetry $y = 0$, i.e., the gap between the root of the wind-tunnel model and the fuselage of the configuration is closed and the wing span runs from the plane of symmetry to the wing tip.

For the wind-tunnel model the axis of rotation of the flapping motion is located at a distance of 0.04 m from the plane of symmetry of the configuration. For the simplified configuration the axis of rotation of the flapping motion of the wing is located in the plane of symmetry, i.e., along the *x*-axis.

B. Parameters of Flapping-Wing Motion

The present Unsteady Lifting-Line Method has been applied to simulate the flow about the flapping wing of the wind-tunnel model of the Robird [19, 21, 22]. The wind-tunnel model has been tested for a number of sets of kinematic parameters for a few combinations of free-stream conditions. Table 2 provides a list of values of the parameters for which computational results have been obtained. Note that the flapping frequency f Hz and free-stream velocity U_∞ m/s are combined, with the excursion of the wing tip $2h_0$ (which is proportional to γ_0) in the Strouhal number St., see Eq. (8b). The experiments focus on St = 0.19, 0.24 and 0.3343.

Table 2 Flapping wing parameters used in wind-tunnel tests.

γ_1	7.5 deg	$2h_0(\lvert y\rvert/0.5b = 1)$	0.67 m
γ_0	34.2 deg	St	0.001, 0.01, 0.025, 0.05, 0.1, 0.15, 0.19, 0.24, 0.3, 0.3343, 0.4
θ_1	0		
θ_0	0(2.5)20 deg		
ϕ	90 deg		

Dimension analysis shows that, using $(\rho_\infty, U_\infty, b)$, the dimensionless aerodynamic properties A of the flapping wing motion can be expressed as $A = A(St, \theta_0, \gamma_1, \theta_1, \phi, \text{AR})$ and airfoil characteristics a_0 and α_0. In the present study the focus is on the dependency of the aerodynamic properties on the amplitude of the pitching motion θ_0 and on the Strouhal number St.

C. Discretization flapping-wing configuration

For the purpose of application of the present Unsteady-Lifting-Line method to the simplified flapping-wing configuration, the linearized (transpiration type of) boundary conditions are imposed on a rectangular domain of span b and chord $\bar{c}$ in the plane $z = 0$, but, the effect of varying chord $c(y)$ is retained in the formulation. The free-stream velocity is parallel to this plane, directed in positive *x*-direction ($\alpha = 0$).

The lifting line of the simplified flapping-wing configuration is located along the quarter-chord line ($x = 0, y \in [-b/2, b/2], z = 0$). The trailing edge (TE) is located at ($x = 3\bar{c}/4, y \in [-b/2, b/2], z = 0$). The lifting line is divided into $N = 80$ elements, here in a uniform distribution. The chord $c(y)$ of the airfoil sections and the effective angle of attack $\alpha_{eff}(y,t)$ are assigned to the mid-points (collocation points) of the N elements on the lifting line. The circulation $\Gamma_{c/4}(y,t)$ of the lifting line is discretized by element-wise, central, quadratic representations $f(y)$ based on $\Gamma_{c/4}(y,t)$, at three consecutive collocation points: $y = y_{k-1}, y_k$ and y_{k+1}, with $\Gamma_{c/4}(y_k,t)$, for $k = 1(1)N$ as unknowns to be determined. In the Unsteady Lifting-Line method the N unknown $\Gamma_{c/4}(y_k,t)$'s are solved for. Across the edges of the elements, the element-wise quadratic representations $f(y)$ are continuous in function value and in first derivative, guaranteeing a continuous, second-order accurate representation of the dipole distribution $\mu(x,y,t)$ on wing and wake.

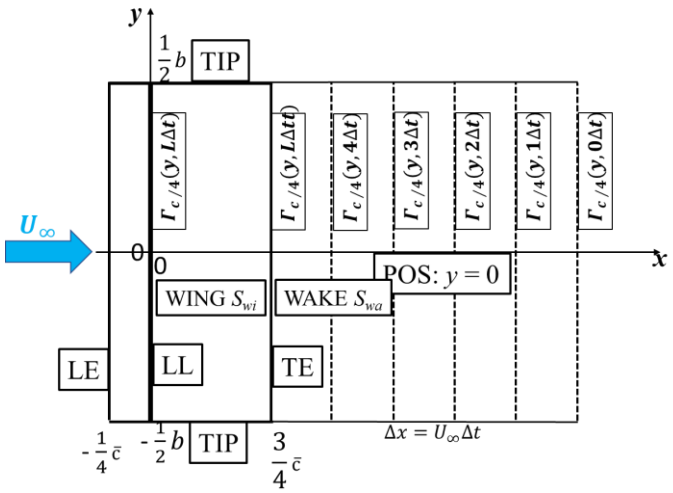

Fig. 8 Time-stepping procedure progressed to time $t = L\Delta t$, L = 5.

Figure 8 shows that between the lifting line at $x = 0$ and the TE at $x = 3\bar{c}/4$, the dipole distribution $\mu(x, y, t) = \Gamma_{c/4}(y, t)$, i.e., $\mu(x, y, t)$ is constant in x-direction, therefore, the discretization consists of a chord-wise strip conveying the circulation of the lifting line (LL) to the trailing edge (TE). The discretization of the wake, situated downstream of the TE, is tied to the time-stepping procedure used to obtain the time-dependent solution. For each new increment Δt in time, the trailing edge of the wake domain is extended by a spanwise strip of width $\Delta x = U_\infty \Delta t$. Then the dipole distribution on the wake is shifted over this distance in downstream direction, such that at time t: $\mu(x, y, t) = \mu(x - U_\infty \Delta t, y, t - \Delta t)$. The number of time steps per period t equals 20, i.e., $\frac{\Delta t}{T} = \Delta\tau = 0.05$. In the present study four full periods of the flapping motion have been simulated, i.e., the calculation comprises 80 time-steps.

V. Results

A. Wake Topology

Figure 9 presents iso-contours of the dipole distribution $\mu(x, y, t = 4T)/(U_\infty \bar{c})$ on the wing and on the wake of the simplified configuration at t/T = 4, i.e., after 4 periods of the flapping/pitching motion, with magnitude in pitching motion of $\theta_0 = 0(2.5)20$ deg. Results are presented for 3 values of the Strouhal number: a high value St = 0.4, an intermediate value St = 0.24 and a low value St = 0.1. This covers the range of Strouhal numbers encountered in bird aerodynamics.

On the wing the instantaneous dipole distribution $\mu(x, y, t = 4T)/(U_\infty \bar{c}]$ is constant in x-direction. On the wake the dipole distribution is clearly periodic in space, with dimensionless spatial period $U_\infty/(fb/2)$, which is proportional to 1/St. Also, the dipole distribution is symmetric with respect to the plane $y = 0$: $\mu(x,-y,t/T) = \mu(x,y,t/T)$. Consequently, the x-component (chordwise) $\gamma_x = -\partial\mu/\partial y$ of the vortex distribution is anti-symmetric: $\partial\mu/\partial y(x,-y,t/T) = -\partial\mu/\partial y(x,y,t/T)$. The y-component (spanwise) $\gamma_y = \partial\mu/\partial x$ of the vortex distribution is symmetric with respect to the plane $y = 0$: $\partial\mu/\partial x(x,-y,t/T) = \partial\mu/\partial x\ (x,y,t/T)$.

The iso-contours of the dipole distribution provide the topology of the wake. Regions with low values of $\mu(x, y, t)$ are blue-coloured, regions with high values of the dipole distributions are red-coloured. Iso-contours of the dipole distribution coincide with vortex lines, see section IV.A and Eq. (14). The closed regions with high (reddish) values of the dipole distribution μ, have the gradient of the dipole distribution, $\vec{\nabla}\mu$, pointing in the direction of the maximum value of $\mu(x, y, t)$. From $\vec{\gamma} = \vec{e}_z \times \vec{\nabla}\mu = -\frac{\partial \mu}{\partial y}\vec{e}_x + \frac{\partial \mu}{\partial x}\vec{e}_y$ it then follows that in the iso-plots, the closed reddish regions represent regions with closed clockwise running vortex lines, forming a ring-like vortical structure in the plane of the wake. The closed bluish regions represent regions with closed anti-clockwise running vortex lines, so is ring-like vortical structure in the plane of the wake of opposite sign.

The regions with high values of $\mu/(U_\infty \bar{c})$ are produced during the downstroke of the wing. The bluish regions with closed, counter-clockwise running vortex lines, are regions with negative values of $\mu/(U_\infty \bar{c})$, also a ring-like

vortex of opposite direction, which are produced during the downstroke of the wing. Locally, the denser the iso-μ lines, the larger $\vec{\nabla}\mu$ and the stronger the vortex distribution.

From the starboard side of the wing, vortex lines start and subsequently proceed in downstream direction. The more outboard starting vortex lines turn around to return to the part of the trailing edge next to the tip. Vortex lines starting from the part of the trailing edge closer to the plane of symmetry (root) do not return to the trailing edge. These vortex lines continue downstream, meandering around a sequence of regions with closed, alternatingly clock-wise and counter-clockwise running, vortex lines.

The sub-plots in Fig. 9, with the spanwise distribution of the effective angle of attack α_{eff} at a number of instants in the cycle of the motion, show clearly that the pitching motion reduces the angle of attach induced by the plunging motion. The latter is linearly proportional to the spanwise coordinate and zero at the plane of symmetry. This shows that for increasing pitch amplitude α_{eff} switches sign, see also Fig. 4.

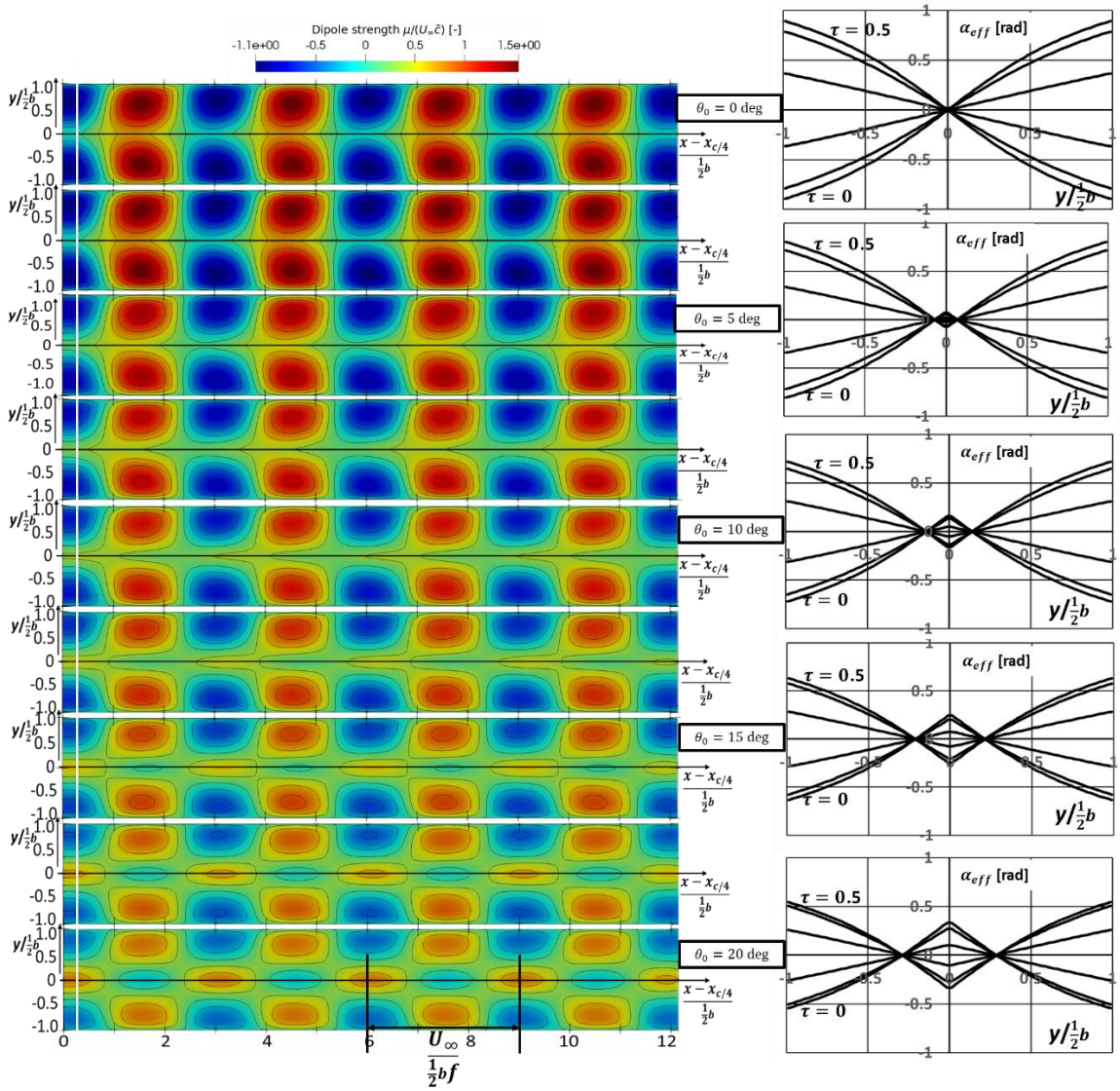

Fig. 9a Iso-contours of dipole distribution on wing and wake of simplified configuration, for conditions listed in Tables 1 and 2, for St = 0.4, θ_0 = 0(2.5)20 deg, N = 80, $\frac{\Delta t}{T} = 0.05$. Flow is from left to right. Iso-contour values range from $\mu/(U_\infty \bar{c}) \in [-0.77, 1.5]$ in ten equal steps. Column on right shows spanwise distribution effective angle-of-attack $\alpha_{eff}(\eta, \tau)$ as function of $\eta = y/0.5b$ and $\tau = t/T$ for every 5 deg increment in pitch angle amplitude θ_0. These sub-figures present the spanwise distribution of $\alpha_{eff}(\eta, \tau)$ for half the upstroke ($\tau \in [0, 0.25]$) followed by half the down stroke $\tau \in [0.25, 0.5]$). Note that at time t, μ at location $x - x_{TE}$ in wake equals $\Gamma_{c/4}(y, t - (x - x_{TE})/U_\infty \bar{c})$. The length of the period of the wake equals U_∞ / f.

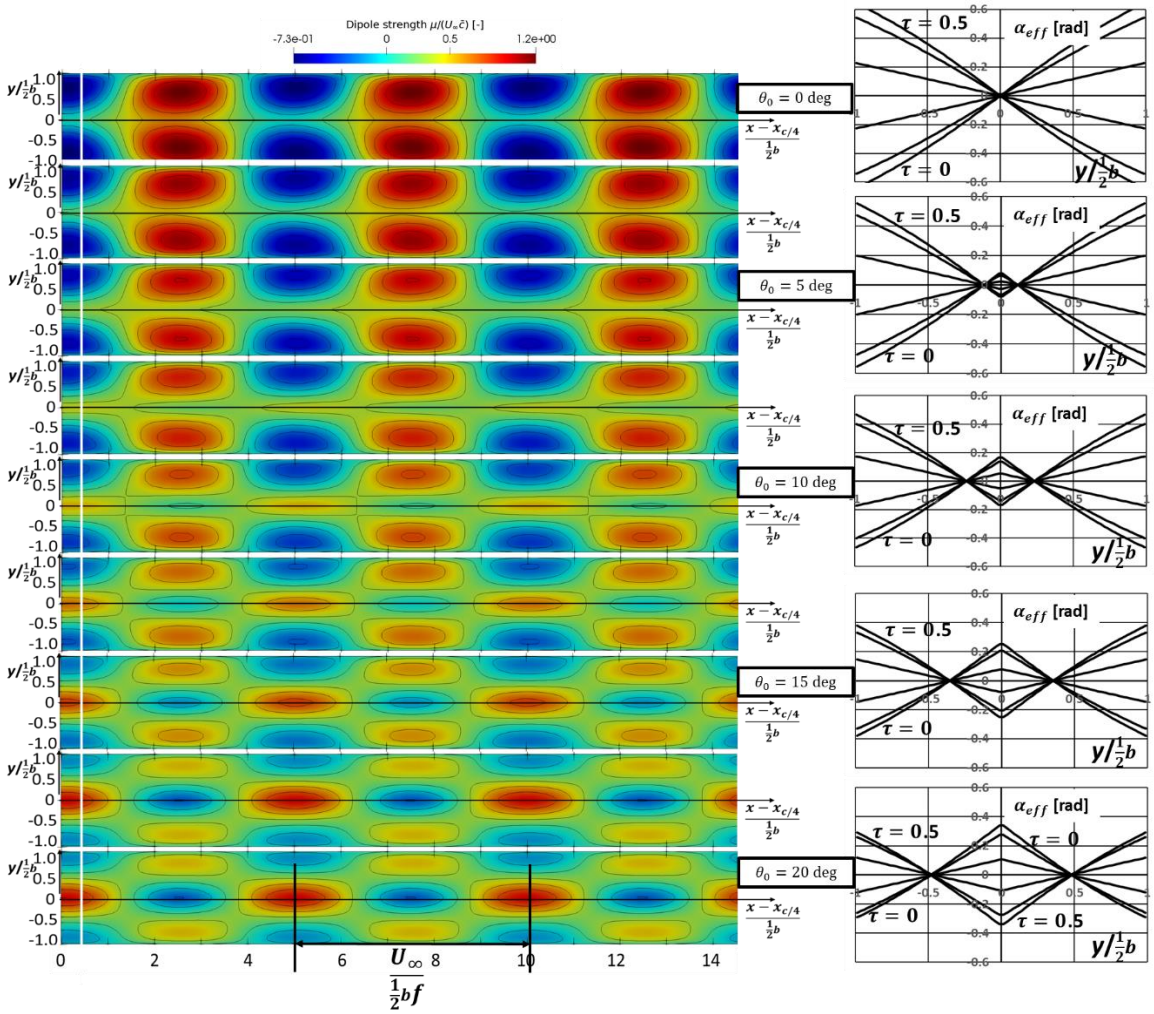

Fig. 9b Iso-contours of dipole distribution on wing and wake of simplified configuration, for conditions listed in Tables 1 and 2, for St = 0.24, θ_0 = 0(2.5)20 deg, N = 80, $\frac{\Delta t}{T} = 0.05$. Iso-contour values range from $\mu/(U_\infty \bar{c}) \in [-0.73, 1.2]$ in ten equal steps. For description, see Fig. 9a.

With increasing pitch amplitude, the spanwise region with inverted α_{eff} increases, which leads to the formation of a wake with 3 vortices rather than two, see Fig 9b. For small Strouhal numbers, the effect of plunging becomes smaller and smaller and pitching dominates the formation of the wake. This result in a third type of wake, with just one ring-like vortex structures stretching along the whole span, of alternating sign in chordwise direction, see Fig. 9c.

For St = 0.1, the period of the wake, equal to $\frac{U_\infty}{f} = 2h_0/St$, is quite long, as is the wake after 4 cycles of the wing motion, therefore, the wake is cut-off at a length of $\frac{x-x_{TE}}{0.5b} = 14.5$.

Figure 9 also illustrates that the spanwise distribution of the effective angle of attack determines the topology of the vortex distribution in the wake. Below a θ_0 of 10 to 12.5 deg, the regions with high, similarly the ones with low, values of the dipole distribution occur in pairs, one region on the starboard side and one equal-signed region on the port-side of the wake. For higher values of the pitch amplitude θ_0, for which in the root part of the wing the effective angle of attack has the opposite sign of the effective angle of attack for the rest of the wing, the weaker and weaker, two equal-signed regions are separated more and more by a region with opposite-signed values of the dipole distribution. For pitch amplitude of θ_0 = 20 deg, the central region of the wing, with opposite-sign dipole distributions are almost as strong as the ones near the wing tips. With increasing pitch amplitudeθ_0 , the vortex wake becomes more complex in topology and the ring-like vortex regions become weaker, which results in lower lift and lower thrust. With decreasing Strouhal number these effects become more pronounced.

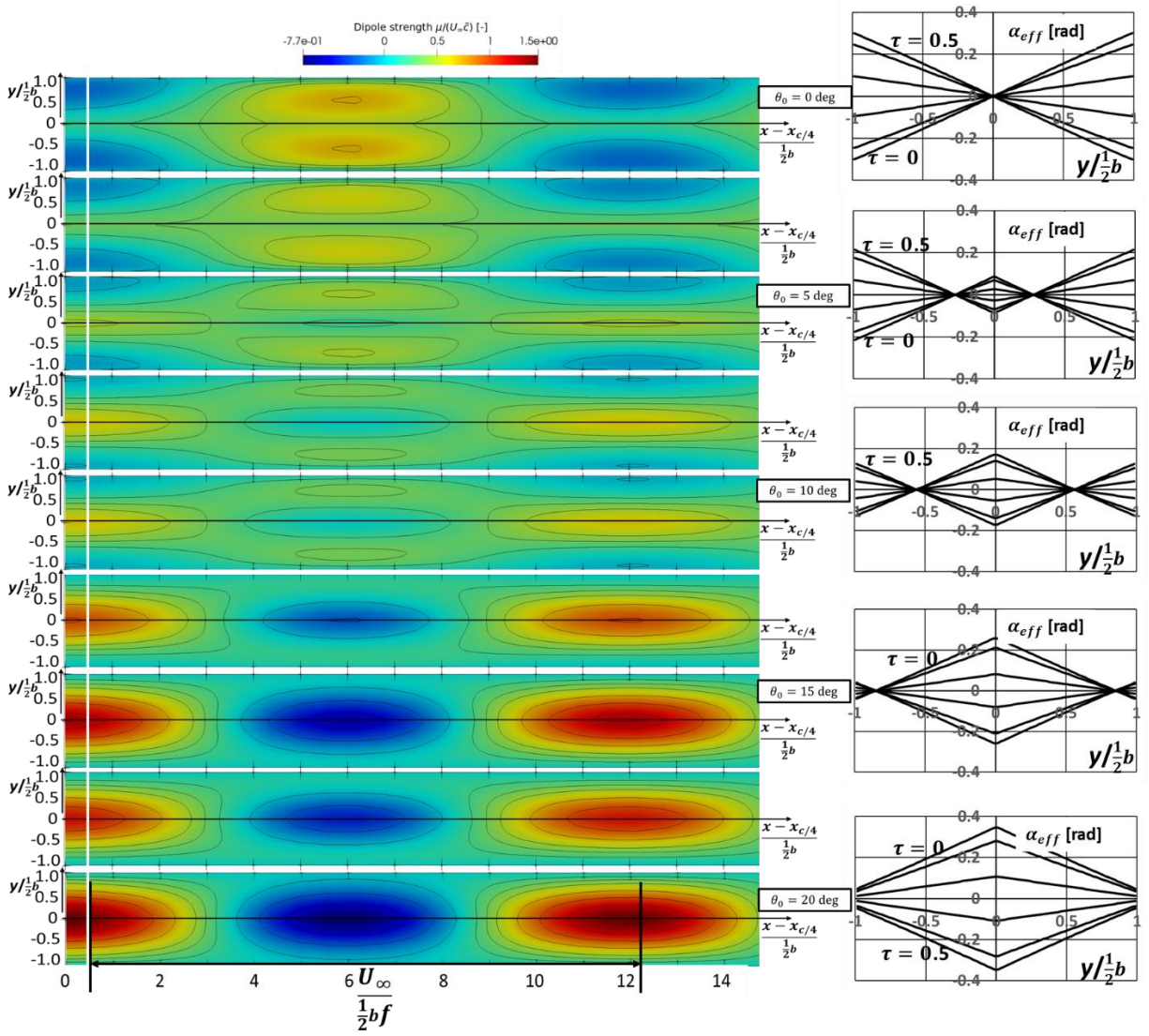

Fig. 9c Iso-contours of dipole distribution on wing and wake of simplified configuration, for conditions listed in Tables 1 and 2, for St = 0.1, $\theta_0 = 0(2.5)20$ deg, N = 80, $\frac{\Delta t}{T} = 0.05$. Iso-contour values range from $\mu/(U_\infty \bar{c}) \in [-0.73, 1.2]$ in ten equal steps. For description, see Fig. 9a.

B. Spanwise Distributions Cycle-Averaged Load and Drag (-Thrust) Coefficients

For St = 0.3343, Fig. 10 presents $\overline{c_\ell(y/(b/2),t)}c(y)/\bar{c}$, the spanwise distribution of the cycle-averaged wing loading (lift) and of $\overline{c_d(y/(b/2),t)}c(y)/\bar{c}$, the cycle-averaged axial (drag) loading, for the whole range of pitch amplitudes $\theta_0 = 0(2.5)20$.deg

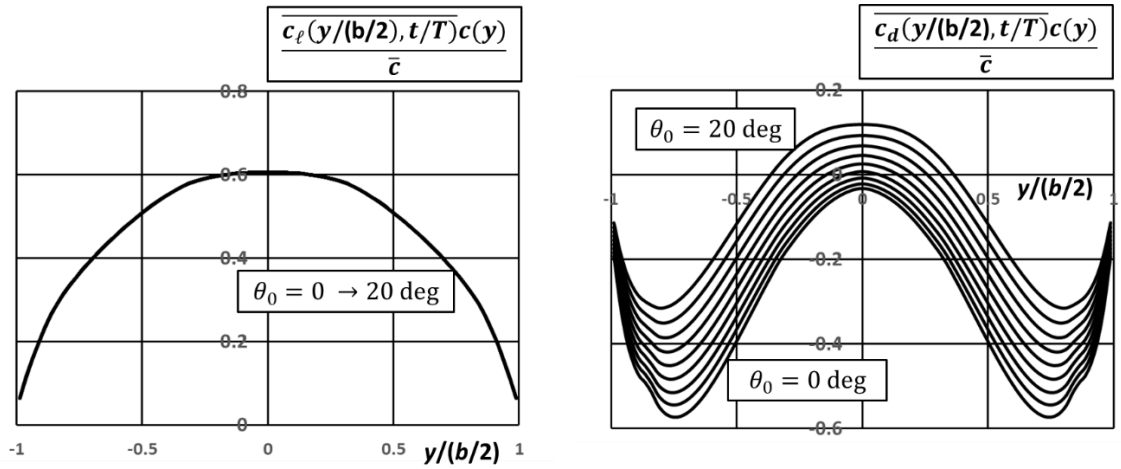

Fig. 10 Left: Spanwise distribution cycle-averaged section wing loading $\overline{c_\ell(y/(b/2),t/T)}c(y)/\bar{c}$. Right: Spanwise distribution cycle-averaged section axial loading $\overline{c_d(y/(b/2),t/T)}c(y)/\bar{c}$. Lifting line method of simplified configuration, for conditions listed in Table 1 and Table 2, St = 0.3343, θ_0 = 0(2.5)20 deg, N = 80, $\frac{\Delta t}{T} = 0.05$.

It is noted that the cycle-averaged values $\overline{f(t)}$ are obtained from the temporal values $f(t)$ by applying the midpoint quadrature rule, for the n-th cycle with I sample points:

$$\overline{f(t)} \equiv \frac{1}{T}\int_{nT}^{(n+1)T} f(t)dt \approx \frac{1}{T}[\frac{1}{2}(t_2 - t_1)f(t_1) + \sum_{i=2}^{I-1}(t_{i+1} - t_i)f(t_i) + \frac{1}{2}(t_I - t_{I-1})f(t_I)], \quad (54)$$

with $t_1 = nT$, $t_I = (n+1)T$ and $\sum_{i=1}^{I-1}(t_{i+1} - t_i) = T$.

The cycle-averaged lift (load) distribution $\overline{c_\ell(y/(b/2),t)}c(y)/\bar{c}$, is highest in the mid-section of the wing, with the distribution decreasing smoothly to zero at the wing tips, in a square-root-type of fashion. The spanwise distribution of the cycle-averaged wing loading does not depend on the pitch amplitude θ_0, only on the Strouhal number. This can be deduced from the formulation of the unsteady lifting-line theory, presented in section III.

Furthermore, the spanwise distribution of the cycle-averaged pitching moment, cycle-averaged circulation $\overline{\Gamma_{c/4}(y/0.5b),t/T)}/U_\infty\bar{c} = 0.5\overline{c_\ell(y/(b/2),t)}c(y)/\bar{c}$, as well as the distribution of the cycle-averaged upwash $\overline{w_{in}(y/0.5b),t/T)}/U_\infty$, only depend on Strouhal number St, not on the pitch amplitude θ_0. This is illustrated in Fig. 11, which presents the data for all combinations of St and θ_0. Both distributions of cycle-averaged quantities do not depend on the pitch amplitude. These results show that the cycle-averaged circulation, and therefore the cycle-averaged wing loading decrease with increasing Strouhal number St.

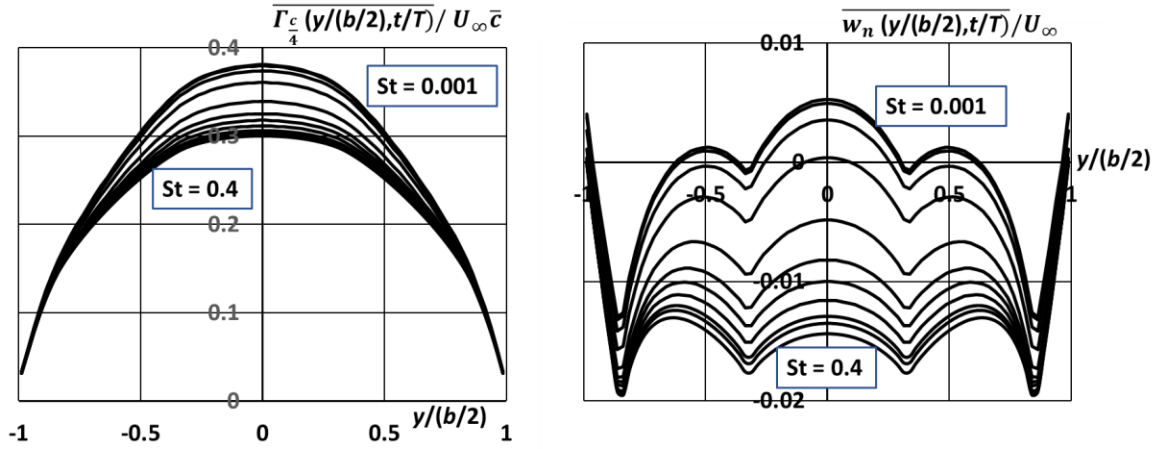

Fig. 11 Left: Spanwise distribution cycle-averaged section circulation $\overline{\Gamma_{c/4}(y/(b/2),t/T)})/U_\infty\bar{c}$. Right: Spanwise distribution cycle-averaged upwash $\overline{w_n(y/(b/2),t/T)}/U_\infty$. Lifting line method of simplified configuration, for conditions listed in Table 1 and Table 2, St = 0.001 to 0.4, θ_0 = 0(2.5)20 deg, N = 80, $\frac{\Delta t}{T} = 0.05$.

For the cycle-averaged upwash, independent of the pitch amplitude θ_0, it illustrates that the cycle-averaged upwash is negative for all Strouhal numbers larger than 0.05.

Fig. 10 shows that the spanwise distribution of the cycle-averaged sectional drag (thrust), involving the product of time-dependent circulation and time-dependent upwash, depends on both Strouhal number St and pitch amplitude θ_0, as can be deduced form Eq. (49). Here, for St = 0.3343, the spanwise distribution of $\overline{c_d(y/(b/2), t/T)}c(y)/\bar{c}$ varies smoothly with pitch amplitude θ_0, at any spanwise location decreasing stepwise with the stepwise pitch amplitude increasing from $\theta_0 = 0$ deg to θ_0 = 20 deg. It appears that, for $\theta_0 < 7.5$ deg, the cycle-average thrust is positive along the whole lifting line, while for higher pitch amplitudes θ_0 an increasing part of the root section is subjected to drag, with a value of 0.12 at the root for $\theta_0 = 20$ deg.

C. Evolution Overall Lift and Thrust Coefficients

For St = 0.3343, Fig. 12 presents the time-dependent lift coefficient $C_L(t)$ and the time-dependent drag (negative of thrust) coefficient $C_D(t)$ of the wing, i.e., the value obtained by integrating the results presented in Fig. 10 with respect to space along the span of the wing. Given the values at the midpoints of the discretisation of the lifting line, the midpoint quadrature rule has been used to obtain the integrated values. Results are shown for the whole range of pitch amplitudes: $\theta_0 = 0(2.5)20$.

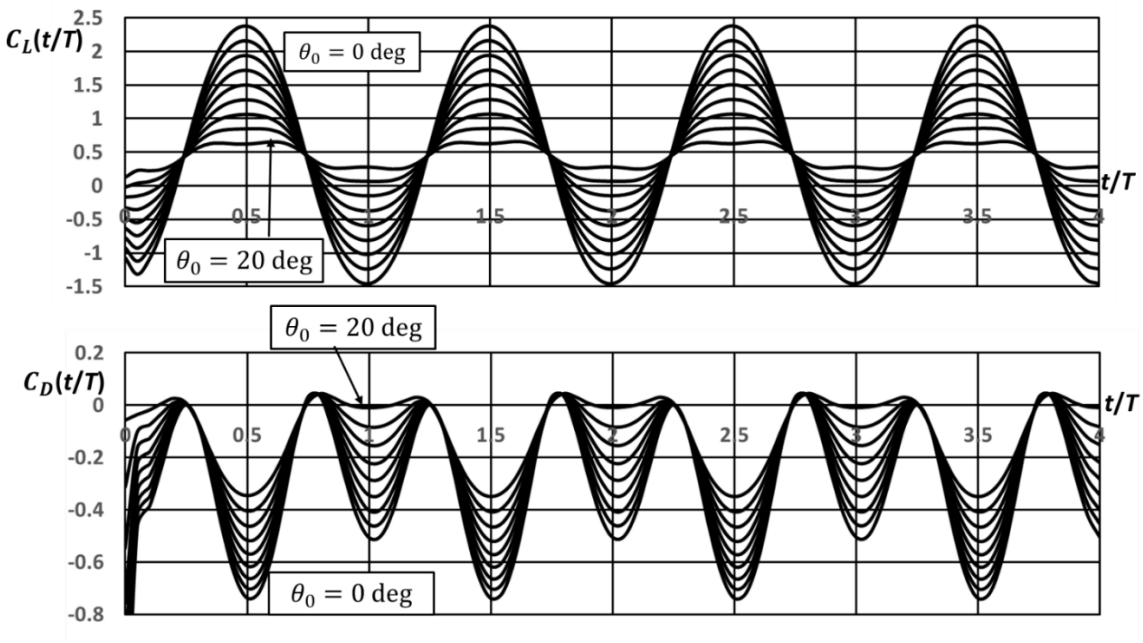

Fig. 12 Upper: Temporal lift coefficient $C_L(t/T)$. Lower: Temporal drag coefficient $C_D(t/T)$. Lifting line method of simplified configuration, for conditions listed in Table 1 and Table 2, St = 0.3343, θ_0 = 0(2.5)20 deg, N = 80, $\frac{\Delta t}{T} = 0.05$.

Both the lift and the drag coefficients become harmonic after the first cycle of the flapping motion. For the lower values of the pitch amplitude θ_0, the amplitude of the lift coefficient is largest, with an amplitude of 2.0 for θ_0 = 0, which decreases with increasing θ_0. For $\theta_0 = 10$ deg this amplitude of the temporal variation of the lift coefficient has decreased to 1.0. For still higher pitch amplitudes, peaks in the temporal distribution flatten out and the variation with time decreases to an amplitude of 0.2. At the highest pitch amplitudes of $\theta_0 > 15$ deg, the lift coefficient is positive during the whole cycle. Note that, though the amplitude of $C_L(t/T)$ very much depends on the pitch amplitude θ_0, like the spanwise distribution of the cycle-averaged wing load. The cycle-averaged value $\overline{C_L}$ of the time-dependent overall lift coefficient $C_L(t)$ does not vary with pitch amplitude θ_0.

The evolution of the drag coefficient is also harmonic, but in a form somewhat more complex than the lift coefficient. This can be understood by realising that the drag is proportional to the product of the distribution of the circulation of the lifting line and the upwash distribution, induced at the lifting line, by the wake dipole distribution. The latter depends linearly on the circulation distribution of the lifting line at the same moment in time and at all earlier moments in time. That yields a first harmonic at double the frequency of the frequency of the flapping/pitching motion [21].

The maximum value of the harmonic drag/thrust coefficient decreases with increasing pitch amplitude: the peak amplitude of the thrust coefficient ($-C_D(t/T)$) equals about 0.7 in absolute value at $\theta_0 = 0$, which decreases to 0.35 at $\theta_0 = 20$ deg

D. Time-Averaged Overall Lift and Thrust coefficients, dependence on θ_0 and St

Figure 13 presents the cycle-averaged lift coefficient $\overline{C_L} = \overline{C_L(t/T)}$ and the cycle-averaged thrust coefficient $\overline{C_T} = -\overline{C_D(t/T)}$ as function of the Strouhal number St, for pitch amplitude θ_0 = 0(2.5)20 deg. The Strouhal numbers considered were St = {10^{-3},10^{-2},0.025,0.05,0.1,0.15,0.19,0.24,0.3,0.3343,0.4}. Figure 13 shows that the unsteady-lifting-line method predicts a mean lift coefficient that, like the cycle-averaged load distribution, does not depend on the pitch amplitude. For small values of St the lift coefficient asymptotes to $\overline{C_L}$ = 0.5507, the drag coefficient to $\overline{C_D}$ = -0.0003. For steady flow, lifting-line theory provides the lift coefficient for an AR = 7.3358 wing with $\alpha_0 = -5$ deg, at zero angle of attack, from [26]:

$$C_L = \frac{a_0}{1+\frac{a_0}{\pi e AR}}(\alpha - \alpha_0),$$

with $a_0 = 2\pi$ the sectional lift slope and e the span efficiency. For e = 1, it follows that $C_L = 0.5483$, a value close to $\overline{C_L}$ = 0.5507 determined in Fig. 13 for St → 0. For the induced drag coefficient $C_{D,in}$, the lifting-line theory provides [26]:

$$C_{D,in} = \frac{C_L^2}{\pi e AR}.$$

So, for the present wing it follows $C_{D,in} = 0.0131$. Figure 13 gives for St = 10^{-3} a value of $\overline{C_D}$ between -0.00014 and – 0.0014, i.e., a small thrust rather than a drag.

The overall lift coefficient $\overline{C_L}$ decreases with increasing Strouhal number, which is due to the shorter wave length of the time-dependent dipole (vortex) distribution on the wake, which equals $\frac{U_\infty}{f} = \frac{2h_0}{St}$. The upwash w_{in} induced by the wake at the lifting line decreases with decreasing St.

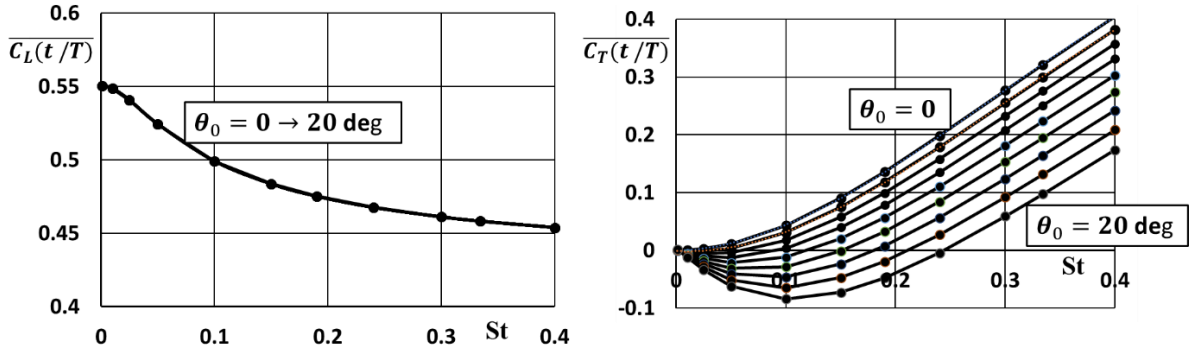

Fig. 13 Left: Mean lift coefficient $C_L = \overline{C_L(t/T)}$ vs Strouhal number St, for pitch amplitude $\theta_0 = 0(2.5)20$ deg. Right: Mean thrust coefficient $C_T = -\overline{C_D(t/T)}$ vs Strouhal number St, for pitch amplitude $\theta_0 = 0(2.5)20$ deg. St = {10^{-3},10^{-2},0.025,0.05,0.1,0.15,0.19,0.24,0.3,0.3343,0.4}. Lifting line method of simplified configuration, for conditions listed in Tables 1 and Table 2, θ_0 = 0(2.5)20 deg, N = 80, $\frac{\Delta t}{T} = 0.05$.

Finally, included in Fig. 13 is the overall, cycle-averaged, thrust coefficient $\overline{C_T}$ as function of Strouhal number St, for the full range of pitch amplitudes θ_0. The results show that the cycle-averaged (mean) span-integrated thrust coefficient is positive for higher Strouhal numbers and lower pitch amplitudes θ_0. There is also a range of combinations (St, θ_0) for which the overall thrust turns into drag: the lower St, the lower the pitch amplitude should be in order to retain thrust.

E. Time-Averaged Required Power Coefficient and Propulsion Efficiency

The curves C_T (St; θ_0), for constant pitching amplitude θ_0,in the range $\theta_0 \in [0,20]$ deg, pass through C_T (St = 0) = 0 and through C_T (St = St_1; θ_0) = 0.
The trendline function of Excel gives an excellent cubic-polynomial-fit

$$C_T(\mathrm{St};\ \theta_0) = a_0(\theta_0) + a_1(\theta_0)\mathrm{St} + a_2(\theta_0)\mathrm{St}^2 + a_3(\theta_0)\mathrm{St}^3, \text{ for St} \in [0,0.4],$$

with consistently a small value of a_0, consistent with the curves passing through the origin, so we chose:

$$C_T(\mathrm{St};\ \theta_0) = \mathrm{St}[a_1(\theta_0) + a_2(\theta_0)\mathrm{St} + a_3(\theta_0)\mathrm{St}^2],$$

with $a_i(\theta_0)$, i = 1,2,3 values found from the Excel trendlines for each θ_0 considered.
Then, it the cubic curve intersecting the St-axis at some θ_0-dependent location $\mathrm{St} = \mathrm{St}_1$, which is calculated from

$$\mathrm{St}_{1,2}(\theta_0) = \frac{-a_2 \pm \sqrt{a_2^2 - 4a_1a_3}}{2a_3}$$

The -sign gives the value of St_1 in the required range of the curves, i.e., St ∈ [0,0.4], for the pitching amplitude in the range $\theta_0 \in [0,20]$deg, in steps of 2.5 deg. Using Excel, adequate low-order polynomial fits are found for both $\mathrm{St}_1(\theta_0)$ and $\mathrm{St}_2(\theta_0)$. Thus, the polynomial fit for the thrust coefficient C_T is expressed, with $A_T(\theta_0) = a_3(\theta_0)$, $\mathrm{St}_{T,1}(\theta_0) = \mathrm{St}_1(\theta_0)$ and $\mathrm{St}_{T,2}(\theta_0) = \mathrm{St}_2(\theta_0)$ as

$$C_T(\mathrm{St};\ \theta_0) = A_T(\theta_0)\mathrm{St}[\mathrm{St} - \mathrm{St}_{T,1}(\theta_0)][\mathrm{St} - \mathrm{St}_{T,2}(\theta_0)],$$

for St ∈ [0,0.4] and $\theta_0 \in [0,20]$deg, with

$$A_T(\theta_0) = -5.1788 - 0.1489\theta_0 - 0.0035\theta_0^2,$$
$$\mathrm{St}_{T,1}(\theta_0) = -0.0103 + 0.0013\theta_0 \text{ and}$$
$$\mathrm{St}_{T,2}(\theta_0) = 0.876 - 0.0091\theta_0.$$

The required power coefficient C_P turns out to be a cubic-polynomial function of the Strouhal number as well. A similar procedure as derived for the thrust coefficient results for the required power coefficient in:

$$C_P(\mathrm{St};\ \theta_0) = A_P(\theta_0)\mathrm{St}[\mathrm{St} - \mathrm{St}_{P,1}(\theta_0)][\mathrm{St} - \mathrm{St}_{P,2}(\theta_0)],$$

for St ∈ [0,0.4] and $\theta_0 \in [0,20]$deg, with

$$A_P(\theta_0) = -3.1487 - 0.0654\theta_0 - 0.0004\theta_0^2,$$
$$\mathrm{St}_{P,1}(\theta_0) = -0.0066 + 0.0011\theta_0 \text{ and}$$
$$\mathrm{St}_{P,2}(\theta_0) = 1.8592 - 0.0034\theta_0 + 0.0003\theta_0^2.$$

The propulsive efficiency $\eta(\mathrm{St};\theta_0)$ is defined as

$$\eta(\mathrm{St};\theta_0) \equiv \frac{C_T(\mathrm{St};\theta_0)}{C_P(\mathrm{St};\theta_0)} = \frac{A_T(\theta_0)[\mathrm{St}-\mathrm{St}_{T,1}(\theta_0)][\mathrm{St}-\mathrm{St}_{T,2}(\theta_0)]}{A_P(\theta_0)[\mathrm{St}-\mathrm{St}_{P,1}(\theta_0)][\mathrm{St}-\mathrm{St}_{P,2}(\theta_0)]}.$$

In the ranges considered both $[\mathrm{St} - \mathrm{St}_{T,2}(\theta_0)]$ and $\left[\mathrm{St} - \mathrm{St}_{P,2}(\theta_0)\right]$ are nonzero, so that it follows that the efficiency equals zero at $\mathrm{St} = \mathrm{St}_{T,1}(\theta_0)$ and has an asymptote at $\mathrm{St} = \mathrm{St}_{p,1}(\theta_0) < \mathrm{St}_{T,1}(\theta_0)$.

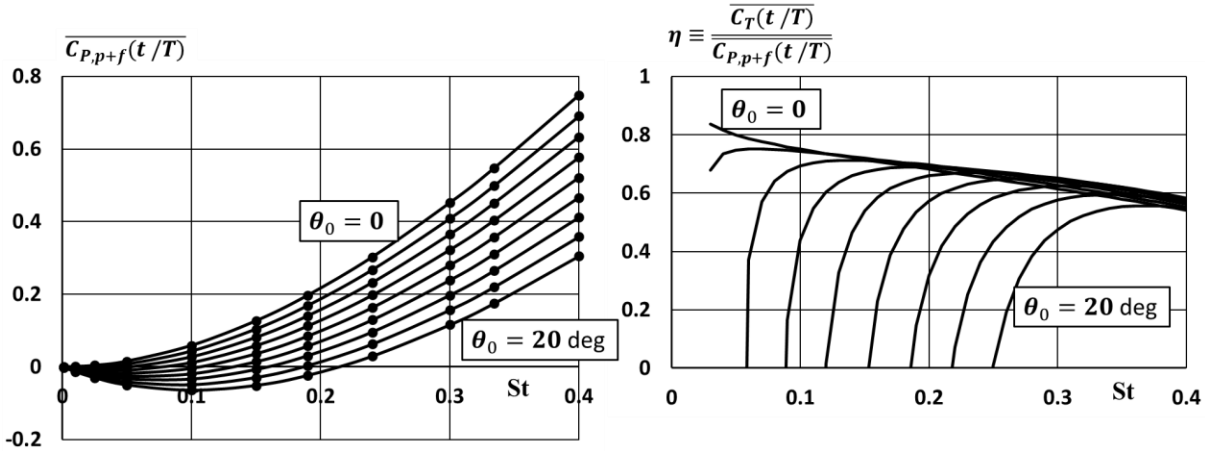

Fig. 14 Left: Mean required power coefficient $C_{P,p+f} = \overline{C_{P,p+f}(t/T)}$ vs Strouhal number St, for pitch amplitude $\theta_0 = 0(2.5)20$ deg. Right: Propulsive efficiency $\eta(St;\theta_0)$ vs Strouhal number St, for pitch amplitude $\theta_0 = 0(2.5)20$ deg. St = {10^{-3},10^{-2},0.025,0.05,0.1,0.15,0.19,0.24,0.3,0.3343,0.4}. Lifting line method of simplified configuration, for conditions listed in Tables 1 and Table 2, θ_0 = 0(2.5)20 deg, N = 80, $\frac{\Delta t}{T} = 0.05$.

Figure 14 shows that the cycle-averaged overall required power coefficient $C_{P,p+f}$ behaves very similarly as the thrust coefficient. In most of the C_T-St plane the power coefficient is positive, only for small values of the Strouhal number and nonzero pitch amplitude, the power coefficient is negative. The resulting propulsion efficiency is highest for lowest pitch amplitude. The propulsion efficiency decreases with increasing Strouhal number.

VI. Conclusions

Prandtl's lifting-line, approximate, theory for the incompressible, inviscid, irrotational, steady flow about thin, mildly-cambered, high-aspect-ratio wings has been extended for application to flapping wings. In the extended theory the circulation of the wing, i.e., of the lifting line, is time-dependent. The theory is formulated in terms of a time-dependent dipole distribution $\mu(x,y,t)$ on a planar, stationary wake reference surface. The planar surface, z = 0, consists of the wing, with attached to its trailing edge, a semi-infinite wake surface also in the plane z = 0.

On the wing the dipole distribution is approximated by a spanwise distribution $\Gamma_{c/4}(y,t)$ along the ¼-chord line, continued to the trailing edge by a chordwise-constant distribution $\mu(x,y,t) = \Gamma_{c/4}(y,t)$. Therefore, the trailing edge carries a dipole distribution identical to the dipole distribution along the lifting line at the 1/4-chord line. This formulation is identical to Prandtl's lifting line formulation, with the lifting-line along the 1/4-chord line, however, with the difference that in Prandtl's theory for steady flow, the chord-wise-constant dipole distribution is continued to infinity downstream. The dipole distribution on the wake surface is the continuation of the dipole distribution on the wing. In the case of unsteady flow, at time *t*, the wake dipole distribution is determined in terms of $\Gamma_{c/4}(y,t^*)$ generated at the trailing edge at earlier times, which subsequently is convected onto the wake surface. The unsteady-lifting-line method includes the newly derived Kutta-Joukowski Theorem for unsteady flow and the Kutta trailing-edge condition for unsteady flow.

The resulting unsteady lifting-line method has been applied to a flapping wing like the Robird wing. The method predicts: (i) the topology of the vortical wake of the flapping wing; (ii) the spanwise distributions of transient (and cycle-averaged) sectional lift (wing load) and sectional axial force (thrust), as well as sectional pitching moment; (iii) the spanwise distributions of transient (and cycle-averaged) sectional required power; (iv) the transient (and cycle-averaged) overall lift, overall thrust and require power, for a number of pitching amplitudes and a number of Strouhal numbers

These numerical results provide insight in the trends in topology of the vortical wake, lift and thrust experienced by the flapping wing due to variation in pitch amplitude and Strouhal number. It has been demonstrated that the spanwise distribution of cycle-averaged sectional circulation, sectional lift (load) and upwash, as well as cycle-averaged overall lift, depend on Strouhal number St, but do not depend on pitch amplitude θ_0, while the spanwise distribution of cycle-averaged sectional thrust and of cycle-averaged overall thrust depend on both Strouhal number and pitch amplitude θ_0. The computational method also predicts the required power and of propulsive efficiency of flapping flight.

References

[1] Folkertsma GA, Straatman W, Nijenhuis N, Venner CH and Stramigioli S. Robird: a robotic bird of prey. *IEEE Robotics and Automation Magazine*, Vol. 24, No. 3, pp. 22–29, 2017. https://doi.org/10.1109/MRA.2016.2636368.

[2] Gerdes J, Holness A, Perez-Rosado A, Roberts L, Greisinger A, Barnett E, Kempny J, Lingam D, Yeh CH, Bruck HA and Gupta SK. Robo Raven: A flapping-wing air vehicle with highly compliant and independently controlled wings. *Soft Robotics*, Vol. 1, No. 4, pp. 275–288, 2014. https://doi.org/10.1089/soro.2014.0019.

[3] Send W, Fischer M, Jebens K, Mugrauer R, Nagarathinam A, and Scharstein F. Artificial hinged-wing bird with active torsion and partially linear kinematics. *28th Congress of the International Council of the Aeronautical Sciences 2012, ICAS*2012, Vol. 2, pp. 1148–1157, 2012.

[4] Karasek M, Muijres FT, Wagter CD, Remes BD and de Croon GC. A tailless aerial robotic flapper reveals that flies use torque coupling in rapid banked turns. *Science*, Vol. 361, No. 6407, pp. 1089–1094, 2018. https://doi.org/10.1126/science.aat0350.

[5] Wood RJ, The first takeoff of a biologically inspired at-scale robotic insect. *IEEE Transactions on Robotics*, Vol. 24, No. 2, pp. 341–347, 2008. https://doi.org/10.1109/TRO.2008.916997.

[6] Thielicke W, Kesel A and Stamhuis E. Reliable force predictions for a flapping-wing micro air vehicle: A "vortex-lift" approach. *International Journal of Micro Air Vehicles*, Vol. 3, No. 4, pp. 201–215, 2011. https://doi.org/10.1260/1756-8293.3.4.201.

[7] Hubel TY, Hristov NI, Swartz SM and Breuer KS. Time-resolved wake structure and kinematics of bat flight. *Experiments in Fluids*, Vol. 46, No. 5, pp. 933–943, 2009. https://doi.org/10.1007/s00348-009-0624-7.

[8] Muijres FT, Johansson LC and Hedenström A. Leading edge vortex in a slow-flying passerine. *Biology Letters*, Vol. 8, No. 4, pp. 554–557, 2012. https://doi.org/10.1098/rsbl.2012.0130.

[9] Jones KD, Dohring CM and Platzer M F. Experimental and computational investigation of the Knoller-Betz effect. *AIAA Journal*, Vol. 36, No. 7, pp. 1240–1246, 1998. https://doi.org/10.2514/2.505.

[10] Rayner, J. M. V., "A vortex theory of animal flight. Part 1. The vortex wake of a hovering animal," *Journal of Fluid Mechanics*, Vol. 91, No. 4, 1979, pp. 697–730. URL https://www.cambridge.org/core/product/identifier/S0022112079000410/type/journal_article.

[11] Spedding G. The wake of a Kestrel (Falco Tinnunculus) in flapping flight. *Journal of Experimental Biology*, Vol. 127, No. 1, pp. 59–78, 1987.

[12] Li J and Wu ZN. Unsteady lift for the Wagner problem in the presence of additional leading/trailing edge vortices. *Journal of Fluid Mechanics*, Vol. 769, pp. 182–217, 2015. https://doi.org/10.1017/jfm.2015.118.

[13] Mulder JL, Hoeijmakers HWM. Computational and experimental investigation into flapping wing propulsion. *Proceedings 54th AIAA Aerospace Sciences Meeting, AIAA Science and Technology Forum and Exhibition (SciTech*2016*)*, San Diego, California, USA, AIAA Paper 2016-0802, 33 pages, 2016.

[14] Brentjes A, Hoeijmakers HWM. Experimental investigation into wake flapping wing robotic bird. *Proceedings AIAA AVIATION* 2017, 35th *AIAA Applied Aerodynamics Conference*, Denver, Colorado, USA, AIAA Paper 2017-3409, 25 pages, 2017.

[15] Gijsman F, Hoeijmakers HWM. Experimental study of flow in wake robotic bird. *Proceedings AIAA AVIATION Forum*, 2018 *Applied Aerodynamics Conference*, Atlanta, Georgia, USA, AIAA Paper 2018-3175, 18 pages, 2018.

[16] Spedding GR, Rosén M and Hedenström A. A family of vortex wakes generated by a thrush nightingale in free flight in a wind tunnel over its entire natural range of flight speeds. *Journal of Experimental Biology*, Vol. 206, No. 14, pp. 2313–2344, 2003. https://doi.org/10.1242/jeb.00423.

[17] Gutierrez E, Quinn DB, Chin DD and Lentink D. Lift calculations based on accepted wake models for animal flight are inconsistent and sensitive to vortex dynamics. *Bioinspiration and Biomimetics*, Vol. 12, No. 1, 2017. https://doi.org/10.1088/1748-3190/12/1/016004.

[18] Hartman SA, Hoeijmakers HWM, Musters R. Experimental investigation of flow about wing of robot bird. *Proceedings 50th AIAA Aerospace Sciences Meeting including the New Horizons Forum and Aerospace Exposition*, Nashville, TN, USA, AIAA Paper 2012-0055, 19 pages, 2012.

[19] Groot Koerkamp L, de Santana LD, Hoeijmakers HWM, Venner CH. Investigation into wake of flapping wing of robotic bird. *Proceedings AIAA AVIATION Forum*, 2019 *Applied Aerodynamics Conference*, Dallas, Texas, USA, AIAA Paper 2019-3582, 22 pages. eISBN: 978-1-62410-589-0, 2019.

[20] de Santana LD, Sanders MP, Venner CH and Hoeijmakers HWM. The UTwente aeroacoustics wind tunnel upgrade. *Proceedings AIAA AVIATION Forum*, 2018 *AIAA/CEAS Aeroacoustics Conference*, Atlanta, Georgia, USA, AIAA Paper 2018-3136, 12 pages, 2018.

[21] Groot Koerkamp L, de Santana LD, Hoeijmakers HWM, Venner CH. Development and experimental validation of lifting-line-based model for a robotic bird. *Proceedings AIAA AVIATION Forum*, 2022 *Applied Aerodynamics Conference*, Chicago, Illinois, USA, AIAA Paper 2022-tbd, 22 pages, 2022.

[22] Hoeijmakers, H.W.M., Groot Koerkamp, L.H., de Santana, L.D., Venner, C.H., Stramigioli, S., Mulder, J.L., Brentjes, A., Gijsman. F., and Hartman, S.A.: "Investigation Flapping-Flight Aerodynamics of a Robotic Bird," 33rd *Congress of the International Council of the Aeronautical Sciences*, ICAS2022, Stockholm, Sweden, September 4–9, 2022. Paper ICAS 2022-0691.

[23] Huckriede KW, Koop AH, Hospers JM, Hoeijmakers HWM. Finite-volume method with transpiration boundary conditions for flow about oscillating wings. *Conference Proceedings 48th AIAA Aerospace Sciences Meeting*, Orlando, Florida, USA. AIAA Paper 2010-0866, 20 pages, 2010.

[24] Hoeijmakers HWM. Panel methods for aerodynamic analysis and design. *AGARD-FDP/VKI Special Course on Engineering Methods in Aerodynamic Design of Aircraft*. AGARD Report R-783 Chapter 5, 1991.

[25] Prandtl L. Tragflügeltheorie. *Nachrichten der Gesellschaft der Wissenschaften zu Göttingen, Mathematisch-physikalische Klasse*, pp. 451-477, 1918. See also *Application of modern hydrodynamics to aeronautics*. NACA Report No. 116, 1921.

[26] Milne-Thomson LM. *Theoretical hydrodynamics*. 5th edition, Dover Publications, 1968.

[27] Anderson Jr JD. *Fundamentals of aerodynamics*. 6th edition, McGraw-Hill Education,2017.
[28] Katz J. and Plotkin A. Low-Speed Aerodynamics. 2nd edition, Cambridge University Press, 2001. P. 384, Eq. (13.36).
[29] Gies SH., Folkertsma GA., Stramigioli S and Venner CH. Ornithopter flight dynamics: measurement and analysis of the Robird's flapping wing Ornithopter Flight Dynamics: Measurement and Analysis of the Robird's Flapping Wing. http://purl.utwente.nl/essays/74077, 2017.
[30] Westerweel J and Scarano F. Universal outlier detection for PIV data. *Experiments in Fluids*, Vol. 39, No. 6, pp. 1096–1100. https://doi.org/10.1007/s00348-005-0016-6, 2005.
[31] Knoller R. Die Gesetze des Luftwiderstandes. *Flug- und Motortechnik* (Wien), Vol. 3, No. 21, pp. 1– 7.2, 1909.
[32] Betz A. Ein Beitrag zur Erklärung des Segelfluges. *Zeitschrift für Flugtechnik und Motorluftschiffahrt*, Vol. 3, pp. 269–273, 1912.
[33] von Kármán Th and Burgers JM. *Aerodynamic Theory*. Volume II General Aerodynamic Theory - Perfect Fluids. Durand WF (editor-in-chief). Julius Springer, Berlin. 1935. ISBN-13: 978-3-642-89628-6. DOI: 10.1007/978-3-642-91485-0. p. 308, Fig. 105.